UNIVERSITY OF ROME TOR VERGATA

Faculty of Engineering

Engineering Sciences Degree Course

Degree Thesis

Automatic speed reference generators for electric vehicles with in-wheel motors under slip constraints

Supervisor
Verrelli Cristiano Maria

Co-Supervisor
Tiberti Marco

Candidate
Damian Mircea

A.Y. 2016-2017

Three years of study, joys, satisfactions, battles, friendships and despair. It has been a long journey that I have been able to share with so many people. Therefore, it seemed only fair to thank them, because if arrived to this point, it is also because of them.

The most important "Thanks" goes to my parents, who have supported me both economically and emotionally, allowing me to complete this journey.
Thanks to my father, my reference point, who always believed in me, even when I didn't. Thank you for always giving me the strength and the confidence to go on, for making me proud to be your son, every day.
Thanks to my best friend, "my mum", my most trustful counsellor. She has always helped me make the difficult choices, she dried my tears during my defeats, and when needed she would reprehend me so that I would give my best. Before each exam, she always told me: "In bocca al lupo" ("break a leg"), and please, be calm". I found this encouragement very irritating. However, before every exam I always waited for it, because even if I never admitted, it calmed me.
Thanks to my little, but big sister, who despite being my "little girl" is a great woman. Always ready to listen and give me advice. Taking advantage of every situation to try to improve my confidence, teaching me how to walk every day holding my head up high without fear of the judgments of others. Every time I needed her, she was always there for me.
Thanks to all of you, because without you I would never have gotten to the end of this difficult, long and winding journey. I want to dedicate this Thesis to you, my family, my greatest support and my guide.

Special thanks also goes to my Supervisor, Prof. Verrelli Cristiano, first of all for listening and giving me advice on my master degree course, then for giving me such an interesting and ambitious topic, that introduced me to new scientific areas; and also for his availability and support.
For this I'm deeply thankful.

Introduction

In recent years, the automobile industry has been experiencing a considerable transformation. A greater sensitivity of Governments and buyers to topics as consumption, safe driving and environmental pollution has set the foundations for research and innovation to develop more sustainable forms of mobility in terms of emissions and pollution reduction.
In 2008 Tesla Motors, a Californian automobile industry, was the first to meet these requests, re-proposing the introduction in the market of an electric car, with an autonomy of about 340 km and able to reach 200 km/h.
An evolution towards this type of technology can bring not only environmental advantages, such as the reduction in the consumption of petroleum-derived products and, consequently, of emissions, but also technical advantages. The published evidence clearly demonstrates that, at the same power, the torque response of an electric motor is in the order of few milliseconds, which is 10-100 times faster than that of the internal combustion engines [1].
Electric motors are smaller and more compact, facilitating their integration with each vehicle wheel, as shown in figure 1. This technological solution is called In-Wheel motor.

Figure 1: In-Wheel motor arrangement

This implementation was proposed back in 1900, during the World's Fair in Paris, by Jacob Lohner and Ferdinand Porsche (the second was the man who gave his name to the Porsche car company). With the "Lohner-Porsche" System (figure 2), an electric vehicle driven by two In-Wheel motors [33] could reach a speed of 56.3 km/h.

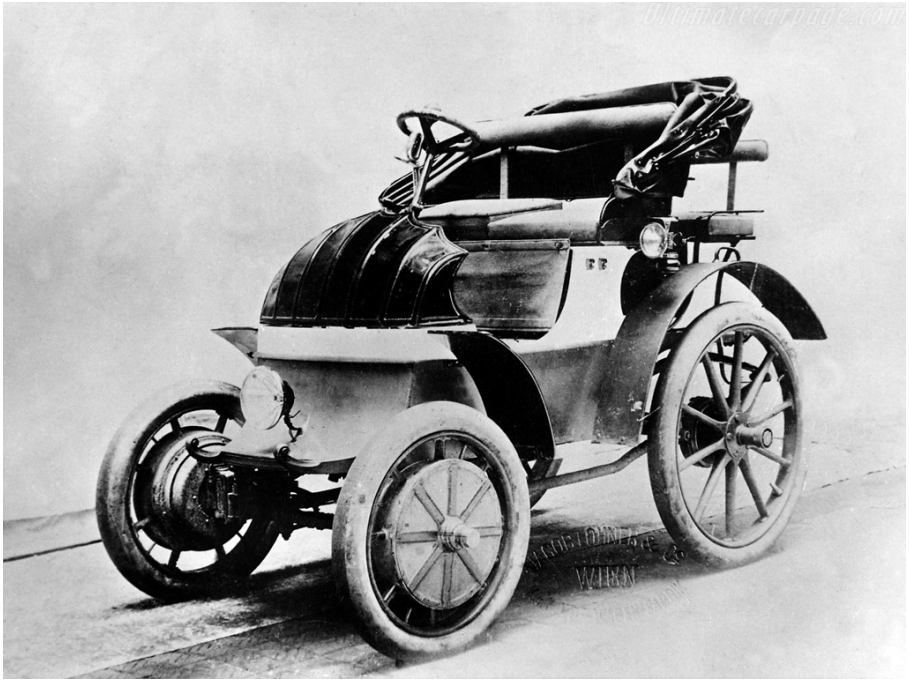

Figure 2: An early 1900s 'System Lohner-Porsche', propelled by in-wheel motors [34]

As previously stated, the use of this technology has considerable technical advantages, due also to the introduction into today's market of very advanced electronic devices, sensors and new materials. Compared to the traditional system, the integration of a motor with each wheel allows the vehicle to have greater flexibility and a higher quality of design. Moreover, the elimination of the entire mechanical transmission produces a reduction of the vehicle weight, increasing the available space, which is used to install independent systems for individual wheel control. This factor ensures better traction and slip control than with other powered systems. A variable torque can be applied to every single wheel during acceleration or braking, compared to the classic "on and off" used by the mechanical ABS system.
Electric motors also have a dual operation, and they can:

- provide energy for traction;
- function as braking generators .

During braking, this allows kinetic energy to be converted into electricity and stored in the battery pack, increasing the vehicle autonomy. Otherwise, this energy would be disperse as heat by the braking system. From energy point of view, the motor and power converter combination allows the achievement of a very high efficiency, over 90%.
However, the biggest restriction of electric vehicles is the power plant (battery pack). In fact, it has high purchase and disposal costs and a short life. In the near future, autonomy could be increased using innovative hybrid strategies.

This dissertation is part of a series of Thesis written by a group of students, and is aimed to the implementation of a control algorithm and to accomplish the experimental set-up that extends the control algorithm proposed in [16] to a two-motor scenario.
The purpose of the control is to regulate the vehicle speed and the yaw rate to guarantee a total safe driving, maintaining the vehicle stability despite the tire-road slip phenomena or, in general, risky external conditions. The experimental results demonstrate the effectiveness of the algorithm while manoeuvring in curves, even with suboptimal road conditions.

Contents

List of Figures

CHAPTER 1

State of art

This chapter describes the state of the art of the problem of the vehicle speed adjustment v to a given constant reference v_*, and its adaptive variations.

1.1 Historical notes

As is known, the number of electronic parts in motor vehicles has enormously increased in recent years: today a high-end car can use up to eighty microcontrollers, not including all the other components needed to complete the systems, such as sensors, drivers or voltage regulators. Only the electronic technologies can enable the automobile industry to meet today's requirements for motor vehicles in terms of safety and reduction of consumption and emissions. Requirements that will become more and more impelling in the near future.
The use of more innovative electronic technology has been a great stimulus for the implementation of new vehicle control algorithms to increase comfort and driving quality. Nowadays, the autonomous driving projects already in the market, as the Tesla Autopilot or the well-known Active Park Assist, have aroused a lot of interest
One of the common problems, typically called "Cruise Control", is to adjust the vehicle speed to a given pre-set speed. The idea of adjusting the vehicle speed has relatively old backgrounds; the first attempt in this direction dates back to 1900, when the British automobile company Wilson-Pilcher introduced on their cars a mechanical device able to regulate the amount of fuel going to the engine in order to guarantee a cruising speed mostly constant. However, the "Modern cruise control", also known as "Tempomat", was proposed for the first time in 1948, by Ralph Teetor, who obtained the patent on the project the same year, under the n^a US 2519859 [35]. From a technical point of view, this system included the use of an electromechanical element (figure 1.1) to regulate the opening of the engine valves according to the rotation speed of the crankshaft.

This new system was incorporated for the first time on the 1958 Chrysler Imperial model.

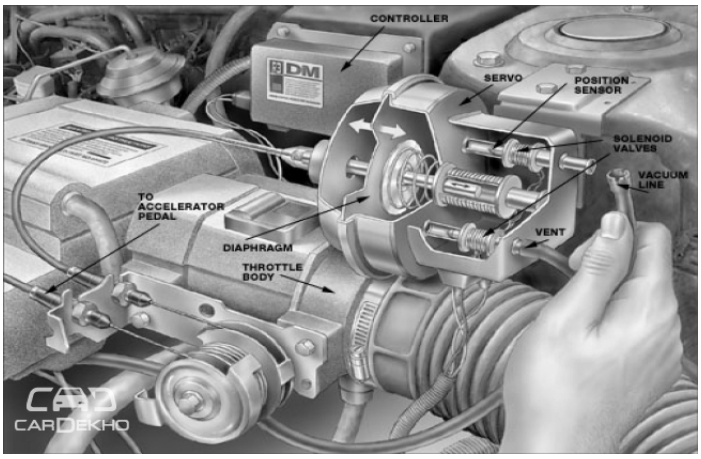

Figure 1.1: Mechanical implementation of the 'modern cruise control'

1.2 Innovation

In the early nineties of the twentieth century, William Chundrlik and Pamela Labuhn proposed an innovative system to regulate the cruise speed, defined as "Adaptive Cruise Control", and in 1995 General Motors [36] filed a patent for this system. Adaptive Cruise Control is a system that allows motor vehicles to adjust autonomously their speed in a busy environment. Radar sensors mounted on the vehicle detects the car is approaching another vehicle ahead, on its path. As in the classic "Cruise control", the driver sets a desired cruising speed; in the event of a slower vehicle is detected ahead, the system decreases the speed in order to maintain a safe distance, a time gap, between the two cars, as in Figure 1.2. If the system detects that the slow vehicle is no longer on its path, then, autonomously, the car accelerates to reach the set cruise control speed.

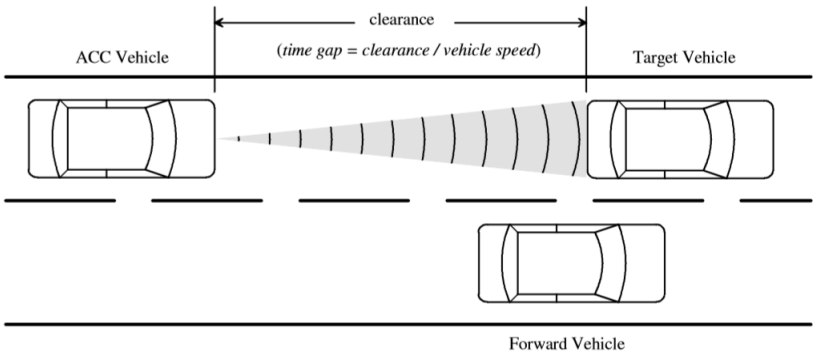

Figure 1.2: Adaptive Cruise Control Vehicle relationships

There are numerous articles about Cruise Control and its variations published in specialized journals. One of those journals is "Transactions on Intelligent Transportation Systems", published by the IEEE (Institute of Electrical and Electronics Engineers). The aim of this publication is to study the so-called ITS (Intelligent Transportation Systems), i.e. systems built on the basis of new technologies and engineering concepts, to develop, improve and promote the coordination and consolidation of the transportation, and to provide a benchmark for cooperation activities.
Inspired by the adaptive observers proposed since the 1980s to the present (presented, among others, in [2-16]), a series of works based on innovative ideas have been developed in the field of the Cruise Control research.

Specifically, in [15] the authors approach the problem of adjusting the longitudinal translation speed of an electric vehicle powered by a single central induction motor. However, for a number of reasons that will be explained in the next chapter, they went from a problem of translation speed regulation to a problem of rotor speed regulation of the vehicle.

Instead, in [16], it is addressed the problem of regulating the vehicle speed to the reference speed, and to adjust the latter in the event of road conditions changes, such as those producing less adherence between tires and road surface, in order to guarantee the passengers' safety. This requirement is made possible using an automatic speed generator for and electric vehicle, powered by a central electric motor, which is autonomously activated when the value of the longitudinal slip between the tires and the road surface is outside the reference values range, defined as safety range.

The objective of this work is the application of the results obtained in [15]-[16] to electric vehicles powered by two in-wheel motors. This technological solution greatly increases the control quality under slip constrains and introduces new possible targets.
The use of two independent electric motors improves the dynamics of the vehicle, compared to the classic one, where an equal torque is applied on right and left wheels and there is a constant distribution between the rear and front axles of the car. From a terminology point of view in vehicles driven by a single internal combustion engine, the control of the torque along the axles of the car, has limited effects during braking so is mainly applied during the traction phase. This limit is exceeded by the use of the two in-wheel motors, which allow not only the use of an independent control on every single wheel during the traction phase and braking but ensures a better vehicle stability during its longitudinal and rotational movements.
The further degree of freedom makes possible to control the translation speed v and the rotational speed adjustment, defined as yaw rate r. Consequently, the risk of slip can be eliminated both during longitudinal and rotational movements, providing that the adjustment of both motors is quickly completed. Moreover, by means of the proposed technological approach, if a trajectory, v_* and r_* can be defined correctly, there is the possibility of implementing autonomous driving algorithms. This advantage has been used to drive the test vehicle and to demonstrate the validity of the proposed algorithms, as will be widely explained later.

CHAPTER 2

Problem definition

This chapter defines the standard Cruise Control architecture for electric vehicles, and later presents the preliminary application of the Cruise Control with rotor speed generator for a central motor. Finally, the case is applied to vehicles equipped with in-wheel motors.

2.1 Cruise Control

The classical architecture of Cruise Controls aims to maintain the vehicle cruising speed to the set speed chosen by the driver, even in the presence of disturbances such as the change of road inclination. The controller, whose inputs are the real speed of the vehicle v and the set cruise control (desired) speed v^*, compensates for changes through a Proportional-Integral (PI) feedback loop about the speed measurement error, generating an output control signal u. This signal will determine the gas flow rate to car engine required to generate a tractive force greater than or equal to the opposite force generated by the vehicle motion of the vehicle.
A schematic diagram of the classic Cruise Control mentioned in [1.1], also called "Tempomat" is presented in figure 2.1.

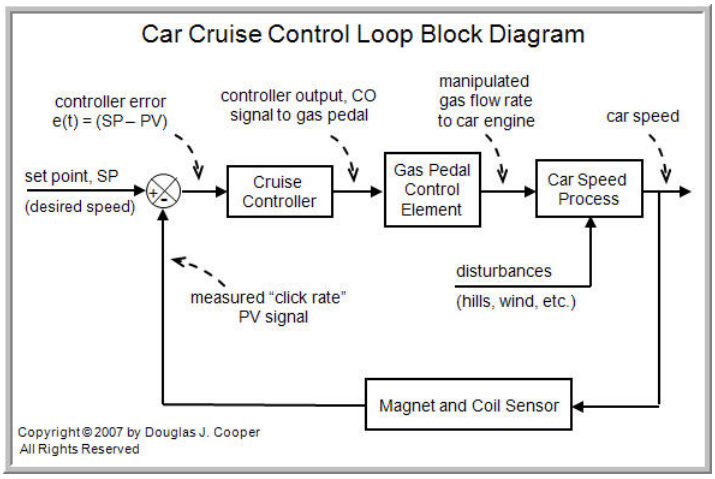

Figure 2.1: Schematic diagram of the classical Cruise Control architecture

The equation of motion of the vehicle is simply:

$$m\frac{dv}{dt} = F - F_d. \tag{2.1.1}$$

The tractive force F is strictly dependent on the torque T, which is proportional to the power generated by the engine and, consequently, to control u and to the wheel rotation speed ω.

$$\omega = \frac{n}{r}v \tag{2.1.2}$$

$$F = \frac{nu}{r}T(\omega) = \alpha_n u T(\alpha_n v). \tag{2.1.3}$$

The disturbance force F_d involves three components: the force of gravity F_g, the rolling friction force F_r, and the aerodynamic drag F_a. The latter can be expressed as:

$$F_g = mg\sin(\sigma) \tag{2.1.4}$$

$$F_r = mgC_r\mathrm{sgn}(v) \tag{2.1.5}$$

$$F_a = \frac{1}{2}\rho C_d A v^2. \tag{2.1.6}$$

where σ is the slope angle of the road, C_r is the coefficient of rolling friction, $sgn(v)$ is the sign of v , ρ the density of the air, C_d the aerodynamic drag coefficient and A the frontal area of the vehicle. Then, the car can be modelled by:

$$m\frac{dv}{dt} = \alpha_n u T(\alpha_n v) - mrC_r sgn(v) - \frac{1}{2}\rho C_d A v^2 - mg\sin(\theta). \tag{2.1.7}$$

The state is the car velocity v, which is also the output. The control signal is the input u, and the latter is defining through a proportional integral, which has the form:

$$u = -k_p\tilde{v} - \int k_i\tilde{v}dt, \tag{2.1.8}$$

where $\tilde{v} = v - v_*$ is the speed error of, and k_p ,k_i are control gains, then the motor vehicle speed regulation to the desired reference speed is guaranteed.

2.2 Cruise Control with rotor speed generator

An evolution of the algorithm previously presented is proposed in [15], where in order to guarantee the implementation of the Cruise Control, a regulation of the rotor speed of a central electric motor is applied. As shown in figure 2.2, a second control loop is added to the classic architecture, whose purpose is to estimate the motor speed rotation ω^*, needed to guarantee the achievement of the desired speed v^*. Based on this estimation, the electromagnetic torque T_e is determined. The innovative control proposed,

- estimates ω^* through a proportional-integral action:

$$\omega_* = \omega_0 - k_p\tilde{v} - k_i \int \tilde{v}dt; \tag{2.2.1}$$

- determines T_e through:

$$T_e = J(-\acute{k}_i \int \tilde{\omega}(\tau)d\tau - \acute{k_p}\tilde{\omega}). \tag{2.2.2}$$

Where J is the moment of inertia, k_p , k_i , $\acute{k_p}$, $\acute{k_i}$, are the gains of the system and $\tilde{\omega} = \omega - \omega^*$ is the rotational speed error of the vehicle. The simultaneous action of these two loops provides a more strong control on cruise speed, compared to classical control, resizing the effect of any exogenous disturbances; (further details on the convergence test can be found in [15]).

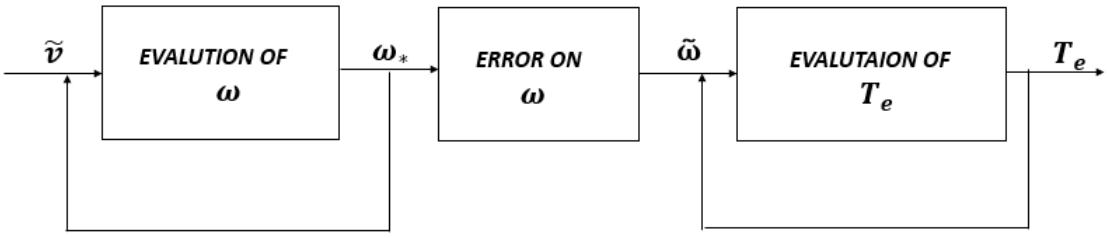

Figure 2.2: Cruise Control scheme for electric vehicles with one induction motor

2.3 Eliminating the sliding risk

In the situation of unfavourable road conditions due to the presence of ice, snow or rain, the use of the previously presented control increases the risk of car slip, defined in common language as hydroplaning. Less grip between the tires and the road could cause an increase of the speed error $\tilde{v}$, resulting that a cruise control functioning according to a classical architecture, would accelerate the vehicle. Yet, this action produces the slip itself. In addition, in some vehicles, the cruise control is deactivated through an intervention on the brake. Under the road conditions described before, the brake activation generates a significant risk factor.
To deal with this significant risk, in [16], the authors offered an innovative approach to the implementation of a cruise control for a vehicle powered by a central electric motor.
The idea is to introduce slip constraints and to evaluate the road conditions moment-by-moment. In the case that the road conditions do not fulfil the set constraint, the estimation generator of ω presented in figure 2.2 is switched off and is replaced by an automatic generator, whose objective is to determine the rotation speed of the motor and, consequently, the new optimal speed v^* for those conditions.
This creates a "control loop", as shown in figure 2.3.

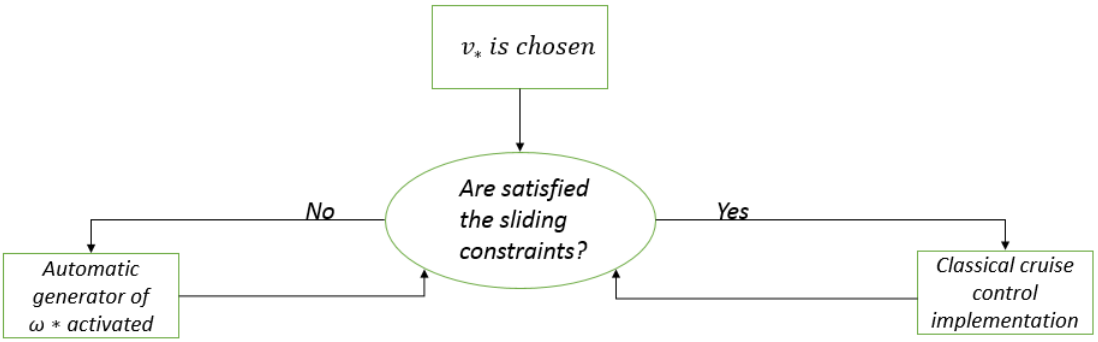

Figure 2.3: Innovative Cruise Control with slip constraints

CHAPTER 3

Cruise Control under Slip Constrains

This chapter introduces the automatic speed reference generator under slip constraints, for a vehicle powered by two in-wheel motors. In the first part, it defines the dynamic model of the vehicle and projects the longitudinal speed and yaw rate controls, without considering the slip. Subsequently, the absence of slip restriction is eliminated, introducing an automatic rotor speed generator, which considers the road conditions.

3.1 Dynamic model of the vehicle

The movement of a motor vehicle, neglecting the rotational dynamics of the wheels, can be defined by equations describing the free motion of a rigid parallelepiped on a flat surface, with one of its faces in direct contact with it.

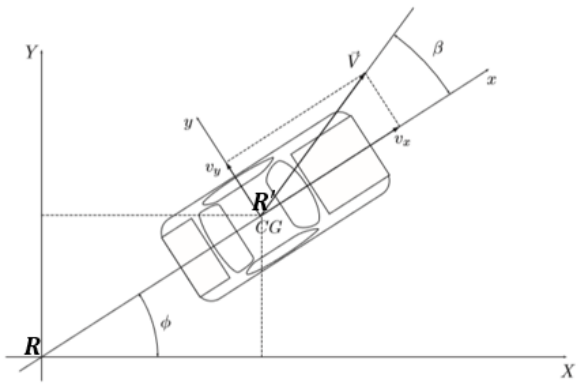

Figure 3.1: Inertial reference frame **R** and reference frame in-built with the vehicle **R'**

Forces and moments acting on the four vertices adhering to the road, due to the interactions with the tires, determine the trajectories. Assuming the absence of suspensions, the motion has three degrees of freedom, and therefore three coordinates are necessary to describe it. In this regard, it is sufficient to use the two reference systems described in figure 3.1. One of those is the inertial reference frame, **R**, and the other, **R'**, the one with its origin at the centre of mass, associated to the vehicle chassis. According to this scheme, the coordinates relative to the translation of the centre of mass are **X** and **Y**, while the angle of rotation is indicated by the yaw angle ϕ.
The vehicle has two in-wheel induction motors for both rear wheels and the steering is applied to the front axle. In reference to figure 3.2, we define the following physical parameter of interest:

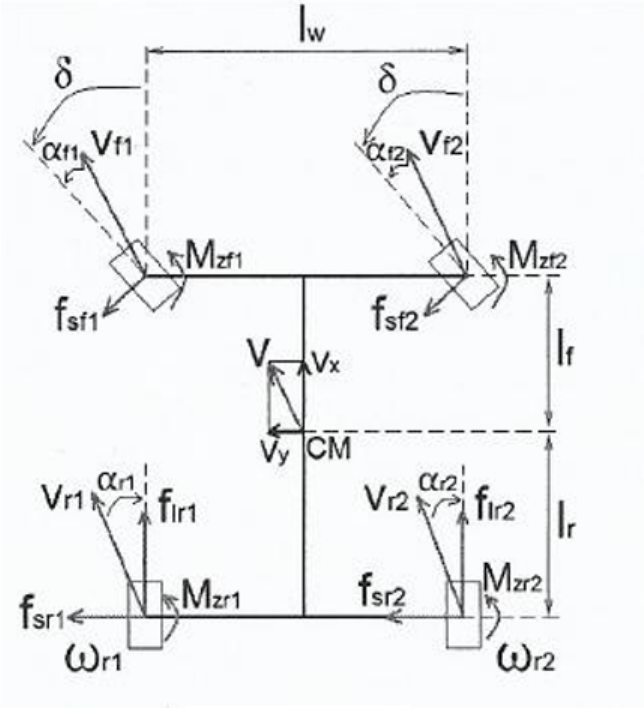

Figure 3.2: Full car model

- v_{ij}: instantaneous speed of centre of mass, $i\epsilon\{f$(front), r(rear)$\}$, $j\epsilon\{l$(left), r(right)$\}$;
- δ steering angle of the wheels, assuming that both are identical, as a simplified hypothesis;
- α_{ij}: tire drift angle between the instantaneous speed direction v_{ij} and the longitudinal direction of the tire, $i\epsilon\{f$(front), r(rear)$\}$, $j\epsilon\{l$(left), r(right)$\}$;
- β_{ij}: angle between the direction of the longitudinal axis of the chassis and the instantaneous speed direction v_{ij}, $i\epsilon\{f$(front), r(rear)$\}$, $j\epsilon\{l$(left), r(right)$\}$;
- f_{ijk}: longitudinal or lateral component of the total force exerted by the road on the tire, $i\epsilon\{s$(side), l(longitudinal)$\}$, $j\epsilon\{f$(front),r(rear)$\}$, $k\epsilon$ $\{l$(left), r(right)$\}$;
- M_{zi}: self-alignment moment applied by the road on the tire. This action brings the longitudinal plane of the wheel to the direction of the speed the vehicle v.

Assuming that the vehicle moves on a flat surface and is performing a roto-translation action from the inertial reference frame to the reference frame having its origin at the centre of mass (or centre-of-momentum) frame, then the dynamics of the vehicle is described by the following nonlinear system of third-order:

$$\dot{v}_x = r v_y + \frac{1}{m}[-(f_{sfl} + f_{sfr})\sin(\delta) - c_a v_x^2] + \frac{1}{m} f_m \tag{3.1.1}$$

$$\dot{v}_y = -r v_x + \frac{1}{m}[-(f_{sfl} + f_{sfr})\cos(\delta) + f_{srl} + f_{srr}] \tag{3.1.2}$$

$$\begin{aligned} \dot{r} &= \frac{l_f}{J_z}(f_{sfl} + f_{sfr})\cos\delta - \frac{l_r}{J_z}(f_{srl} + f_{srr}) + \frac{l_\omega}{2J_z}(f_{sfl} - f_{sfr})\sin(\delta) \\ &+ \frac{1}{J_z}\sum_{J\epsilon\{f_l, f_r, r_l, r_r\}} M_{zj} - \frac{l_w}{2J_z} f_d, \end{aligned} \tag{3.1.3}$$

where v_x e v_y are longitudinal and lateral velocities, respectively; r denotes the yaw rate; the total driving force f_m and the differential force f_d are defined as:

$$f_m = f_{lrl} + f_{lrr} \tag{3.1.4}$$

$$f_d = f_{lrl} - f_{lrr}, \tag{3.1.5}$$

f_{li} is the longitudinal tire force supplied by the two drive wheels, $i\epsilon\{r_l, r_r\}$; m is the total vehicle mass; J_z is the vehicle inertia with respect to the vertical axle passing through the centre of mass; l_f is the distance between the centre of mass and the front axle; l_r is the distance between the centre of mass and the rear-axle; l_w is the width of the vehicle; c_a is the aerodynamics drag coefficient; δ is the steering angle; f_{sj} and M_{zj} are, respectively, the lateral tire force and the self-alignment moment, $j\epsilon\{f_l, f_r, r_l, r_r\}$.
To simulate forces and moments due to the interaction between the tires and the road, the experimental mathematical model of Pacejka is used. This model, also known as the "Magic Formula", is a very empirical model that needs a profound experimental characterization, but has found great success in the field of simulations for its accuracy. The Pacejka model states that the self-alignment moments and the lateral forces (f_{sj} and M_{zj}), are functions of the drift angles α_{ij} and of the longitudinal slip λ_i. These angles are related to vehicle variables and to its physical parameters. A detailed and complete presentation of this model in all its aspects goes beyond the scope of this Thesis; we refer to specific texts [37, 38] for a complete discussion.
The use of the model for the case under analysis, allowed to derive the following equations:

$$f_{li}(\lambda_i) = D_{li}\sin(C_{li}\arctan(B_{li}(1 - E_{li})\lambda_i + E_{li}\arctan(B_{li}\lambda_i))) \tag{3.1.6}$$

$$f_{sj}(\alpha_j) = D_{sj}\sin(C_{sj}\arctan(B_{sj}(1 - E_{sj})\alpha_j + E_{sj}\arctan(B_{sj}\alpha_j))) \tag{3.1.7}$$

$$M_{zj}(\alpha_j) = D_{zj}\sin(C_{zj}\arctan(B_{zj}(1 - E_{zj})\alpha_j + E_{zj}\arctan(B_{zj}\alpha_j))), \tag{3.1.8}$$

characterized by the parameters (B, C, D, E) whose values depend on both the road surface conditions and the normal force acting on the tire.
A phenomenon of high importance is the wheel slip, which can be quantified by defining the parameters of longitudinal sliding or slip λ_i. Considering $R_{\omega i}$ as the radius of the wheel where $i\epsilon\{r_l, r_r\}$, then:

$$\lambda_i = \frac{\omega_i R_{\omega i} - v_i}{v_i}, \tag{3.1.9}$$

with v_i denoting the wheels velocities in the free rolling ideal motion hypothesis, namely:

$$v_{rl} = \sqrt{\left(v_y - r l_r\right)^2 + \left(v_x - r\frac{l_\omega}{2}\right)^2} \tag{3.1.10}$$

$$v_{rr} = \sqrt{\left(v_y - r l_r\right)^2 + \left(v_x + r\frac{l_\omega}{2}\right)^2}. \tag{3.1.11}$$

Ultimately, it is necessary to state the drift angles that are the function of the steering angle and the chosen configuration of the motor vehicle, and they are defined as:

$$\alpha_{fl} = \delta - \arctan\left(\frac{v_y + rl_f}{v_x - r\frac{l_\omega}{2}}\right) \tag{3.1.12}$$

$$\alpha_{fr} = \delta - \arctan\left(\frac{v_y + rl_f}{v_x + r\frac{l_\omega}{2}}\right) \tag{3.1.13}$$

$$\alpha_{rl} = -\arctan\left(\frac{v_y - rl_\omega}{v_x - r\frac{l_\omega}{2}}\right) \tag{3.1.14}$$

$$\alpha_{rr} = -\arctan\left(\frac{v_y - rl_\omega}{v_x + r\frac{l_\omega}{2}}\right). \tag{3.1.15}$$

3.2 Introduction to the algorithm

The previous section presented the dynamic model of the vehicle and the equations that describes its movement. The following parts will introduce the application of the cruise control for a vehicle powered by two independent in-wheel motors. This technological architecture will allow the driver to set a longitudinal cruising speed v_x^*, and a steering angle δ^*. To guarantee the reaching of the reference values, the control will be implemented on the rotation angular speed of the vehicle rear wheels, ω_{rl} and ω_{rr}. That choice ensures more robustness to the algorithm and makes possible to distinguish between the dynamics of the wheels on a straight track, by introducing ω_l, the speed of longitudinal rotation, and the one on a curve, by introducing ω_d, the differential rotation speed. It is necessary to emphasize that the implementation chosen is only possible thanks to the existing independence between the speeds ω_{rl} and ω_{rr}, the same approach is not applicable to a vehicle powered by a central motor, either electrical or with internal combustion engine.
The initial objective will be to derive ω_l and ω_d only knowing v^* and the yaw rate r^*, defined by the knowledge of the steering angle δ^* and the cruising speed, regardless the constraints deriving from the road conditions.
Then, the uncertain parameters μ_i, presented in [16], will be used. These parameters intrinsically incorporate information about the external conditions and it will be demonstrate their close correlation with λ_i . So, in the situation of external conditions causing slip, an automatic rotation speed generator of ω_l and ω_d will be activated, with the purpose to guarantee λ_i values in the safety region.

3.3 Implementation of the control

Let us consider the problem of regulating both the longitudinal speed and the yaw rate in a curve manoeuvre with sufficiently large and constant curvature radius. To obtain a control design, which does not depend on the vehicle model, we assume that the total driving force f_m and the differential force f_d meet the following approximation:

$$f_m = a(v_x, v_y)(\omega_{rl} + \omega_{rr}) - b \tag{3.3.1}$$
$$f_d = a(v_x, v_y)(\omega_{rl} + \omega_{rr}), \tag{3.3.2}$$

with a positive real constant b and a non linear function $a(.)$ of v_x and v_y. From a physical point of view, this approximation implies that:

- the longitudinal slip is negligible, i.e. λ_{rl} e λ_{rr} are relatively small;
- a sufficiently large curvature radius, allowing the speed of the front wheels to be considered equal, $v_{rl} = v_{rr} = v_r$;
- the wheels radii $R_{\omega_{rl}}$ and $R_{\omega_{rr}}$ are equal to each other, namely R_ω;
- the first order truncations of the Maclaurin series of Pacejka models for lateral forces are equal to each other, so that $D_{lrl}C_{lrl}B_{lrl} = D_{lrr}C_{lrr}B_{lrr}$;

The above approximations, even if restrictive, were introduced with the aim of obtaining a simple, theoretically correct, proportional-integral decoupled control and lead to:

$$a(v_x, v_y) = \frac{D_l C_l B_l R_\omega}{v_r(v_x, v_y)} \tag{3.3.3}$$

$$b = D_l C_l B_l. \tag{3.3.4}$$

ω_l and ω_d are here introduced, which respectively indicate the longitudinal and differential components of the angular velocities of the rear wheels defined as (see also [23]):

$$\omega_l = \frac{\omega_{rl} + \omega_{rr}}{2} \tag{3.3.5}$$
$$\omega_d = \omega_{rr} - \omega_{rl}. \tag{3.3.6}$$

Then the equations describing the nonlinear model of the third-order of the vehicle [3.1.(1-3)] can be rewritten as:

$$\dot{v}_x = r v_y + \frac{1}{m}[-(f_{sfl} + f_{sfr})\sin(\delta) - c_a v_x^2] + \frac{1}{m}(2a(v_x, v_y)\omega_l - b) \tag{3.3.7}$$
$$\dot{v}_y = -r v_y + \frac{1}{m}[(f_{sfl} + f_{sfr})\cos(\delta) + f_{srl} + f_{srr}] \tag{3.3.8}$$
$$\dot{r} = \frac{l_f}{J_z}(f_{sfl} + f_{sfr})\cos(\delta) - \frac{l_r}{J_z}(f_{srl} + f_{srr}) + \frac{l_\omega}{2J_z}(f_{sfl} - f_{sfr})\sin(\delta) + \frac{1}{J_z}\sum_{j\epsilon\{f_l, f_r, r_l, r_r\}} M_{zj} + \frac{l_\omega}{2J_z}a(v_x, v_y)\omega_d, \tag{3.3.9}$$

in which the decoupling feature of ω_l and ω_d is emphasised.

For the sake of clarity and compactness, we rewrite the previous model as $(f_x(.), f_y(.), f_r(.), g_x(.), g_r(.))$, which are suitable functions in those variables.

$$\dot{v}_x = f_x(v_x, v_y, r) + g_x(v_x, v_y)\omega_l - \frac{b}{m} \tag{3.3.10}$$
$$\dot{v}_y = f_x(v_x, v_y, r) \tag{3.3.11}$$
$$\dot{r} = f_r(v_x, v_y, r) + g_r(v_x, v_y)\omega_d. \tag{3.3.12}$$

We also introduce the constant reference r^*, which depend on the set cruising speed v_x^* and the steering angle δ^*. This is based on the kinematic relationship (see similar choices in [24] and [25]):

$$r^* = \frac{1}{l_f + l_r}\delta^* v_x^*. \tag{3.3.13}$$

Assuming that there exist two constant references input, ω_l^* and ω_d^* (which are compatible with the constant references output v_x^* and r^*), and a constant reference lateral velocity v_y, the later being uncertain owing to the overall system uncertainties, then we can write:

$$\dot{\tilde{v}}_x = f_x(v_x, v_y, r) + g_x(v_x, v_y)\omega_l - f_x(v_x^*, v_y^*, r^*) - g_x(v_x^*, v_y^*)\omega_l^* \tag{3.3.14}$$
$$\dot{\tilde{v}}_y = f_y(v_x, v_y, r) - f_y(v_x^*, v_y^*, r^*) \tag{3.3.15}$$
$$\dot{\tilde{r}} = f_r(v_x, v_y, r) + g_r(v_x, v_y)\omega_d - f_r(v_x^*, v_y^*, r^*) - g_r(v_x^*, v_y^*)\omega_d^*, \tag{3.3.16}$$

where $\tilde{v}_x = v_x - v_x^*$, $\tilde{v}_y = v_y - v_y^*$ and $\tilde{r} = r - r^*$ are the regulation errors.
At this point, we design the proportional-integral control

$$\omega_l = \frac{v_x^*}{R_\omega} - k_{px}\tilde{v}_x - k_{ix}\int \tilde{v}_x(\tau)d\tau \tag{3.3.17}$$
$$\omega_d = \frac{l_\omega r^*}{R_\omega} - k_{pr}\tilde{r} - k_{ir}\int \tilde{r}(\tau)d\tau, \tag{3.3.18}$$

having as input v_x^* and r^*, variables that can be set by the driver. Thee constants $k_{px}, k_{ix}, k_{pr}, k_{ir}$ are called positive system gains, instead the first terms derive from the assumption previously delineated, i.e. that there exist the values ω_l^*, ω_d^*. These were obtained by the kinematic relationship between radius, rotation speed and translational speed

$$v_x = R_\omega \omega_l \tag{3.3.19}$$
$$r = \frac{R_\omega}{l_\omega}\omega_d. \tag{3.3.20}$$

It describes the motion of a rigid disk on a flat surface, in the absence of any tractors or braking moments. However, in the case of a tire, its veracity is immediately denied by the equation:

$$\lambda_i = \frac{\omega_i R_\omega - v_i}{v_i}. \tag{3.3.21}$$

The equation emphasizes the relationship between the wheels rotation speed and the road conditions, being in fact:

$$\omega_i = \frac{v_i}{R_\omega}(1 + \lambda_i). \tag{3.3.22}$$

If the tire is in motion, the slip cannot be null, and the effective radius does not coincide with the non-deformed radius R_ω or with the one under load, measurable with stopped wheel.
Therefore, the use of the first term only would result in an erroneous definition of the

references. Consequently, it is necessary to introduce a second proportional integral control of the references. Let us define two constants measuring the dynamic deviation, as follows:

$$c_x = \omega_l^* - \frac{v_x^*}{R_\omega} \tag{3.3.23}$$

$$c_r = \omega_d^* - \frac{l_\omega r^*}{R_\omega}, \tag{3.3.24}$$

and the following integral terms whose purpose is to make the error approaching to zero on the uncertain constants c_x, c_r:

$$\tilde{c}_x = -k_{ix} \int \tilde{v}_x(\tau) d\tau - c_x \tag{3.3.25}$$

$$\tilde{c}_r = -k_{ir} \int \tilde{r}(\tau) d\tau - c_r. \tag{3.3.26}$$

Finally, the control can be rewritten as:

$$\omega_l - \omega_l^* = -k_{px}\tilde{v}_x - k_{ix} \int \tilde{v}_x(\tau) d\tau - c_x \tag{3.3.27}$$

$$\omega_d - \omega_d^* = -k_{pr}\tilde{r} - k_{ir} \int \tilde{r}(\tau) d\tau - c_r. \tag{3.3.28}$$

Proof of convergence

Considering the following function of Lyapunov, defined positive:

$$V = \frac{1}{2}(\tilde{v}_x^2 + \tilde{v}_y^2 + \tilde{r}^2) + \frac{g_x(v_x^*, v_y^*)}{2k_{ix}}\tilde{c}_x^2 + \frac{g_r(v_x^*, v_y^*)}{2k_{ir}}\tilde{c}_r^2 \tag{3.3.29}$$

and applying a modification of the local version of the Persistency of Excitation in Lemma [26] to the first-order Taylor expansion to the system defined in [3.3.(13-16)], on point $p = (v_x^*, v_y^*, r^*, \omega_l^*, \omega_d^*)$, we can establish that for sufficiently high gains of k_{px} and k_{pr}, the local exponential convergence to zero of $\tilde{v}_x, \tilde{v}_y, \tilde{r}$ is guaranteed, provided that the (2, 2) element of the Jacobian matrix in the linear approximation of [3.3.(14-16)] is negative.

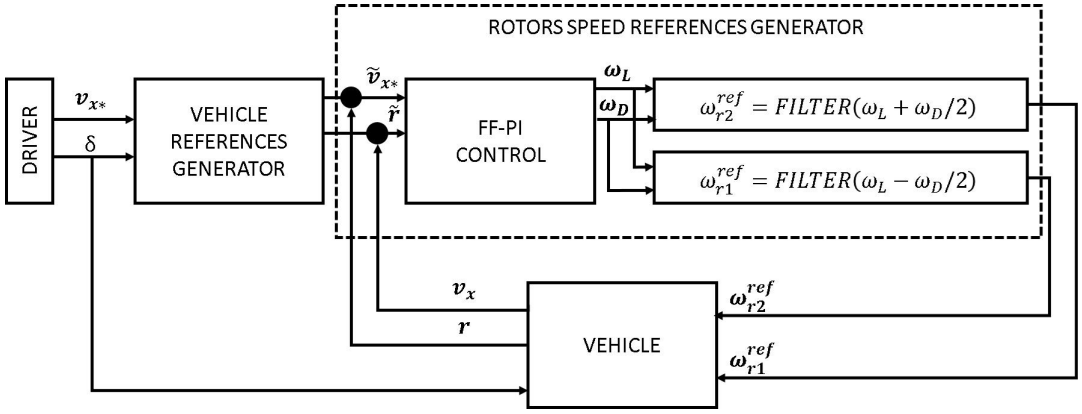

Figure 3.3: Block diagram for the proposed control architecture

The control scheme in figure 3.3 shows the complete architecture of the control, presenting the main designed components together with the involved signals.
The driver sets a constant longitudinal speed value v_x^* and a steering angle δ^*.
The yaw rate is defined in accordance with the two selected parameters. The combination of the FeedFoward/Feedback-Eerror control then allows to generate the proper reference inputs for the rotor speed of each of the two electric motors.

3.4 Slip constraints

To complete the chosen path it is necessary to consider the unpleasant situation of slip. As was repeatedly stated in the previous sections, the final objective is to design an automatic references generator that ensures very low slip values λ_i all into a range defined secure. Now, let us assume that the differential speed ω_d is zero; then, according to the equation [3.3.6], this implies that both rear wheels have the same speed $\omega_{rr} = \omega_{rl}$. Similar scenario is happening during the straight motion.
As in [16], let us move our attention to the rotation speed of the two motor rotors; as they are identical, then named them simply ω and let us introduce the unknown parameters $\mu \epsilon M \subset R^3$, assigning the same values for each one of the driving wheels. These parameters describe the external conditions, such as tire-road adhesion coefficient $\mu_{[1]}$, road slope $\mu_{[2]}$ and the drag force $\mu_{[3]}$.
The derivation of those parameters goes beyond the purposes of this Thesis; for a more complete information, refer to [16]. Let M denote a given compact set [39]:

$$M = \left[\mu_a^{[1]}, \mu_b^{[1]}\right] X \left[\mu_a^{[2]}, \mu_b^{[2]}\right] X \left[\mu_a^{[3]}, \mu_b^{[3]}\right], \tag{3.4.1}$$

where $\left[\mu_a^{[1]}, \mu_b^{[1]}\right]$, $\left[\mu_a^{[2]}, \mu_b^{[2]}\right]$, $\left[\mu_a^{[3]}, \mu_b^{[3]}\right]$ are limit values. In case of slip, the vehicle speed v_x will no longer be linearly dependent on the rotation speed of the wheels. Logically, this linearity is just absent in the case of tire-road slip. It is therefore necessary to assume at priori the existence of the unknown functions $g_{\mu i}(.)$, which report the relationship between ω and v_x, depending on the external conditions.

This means that each of the functions introduced will define a curve in the plane (ω, v); this curve denotes the association between the two velocities in a given scenario. To understand better these notions, refer to figure 3.4, where is represented the dependence between v_x and ω, for different values of μ.

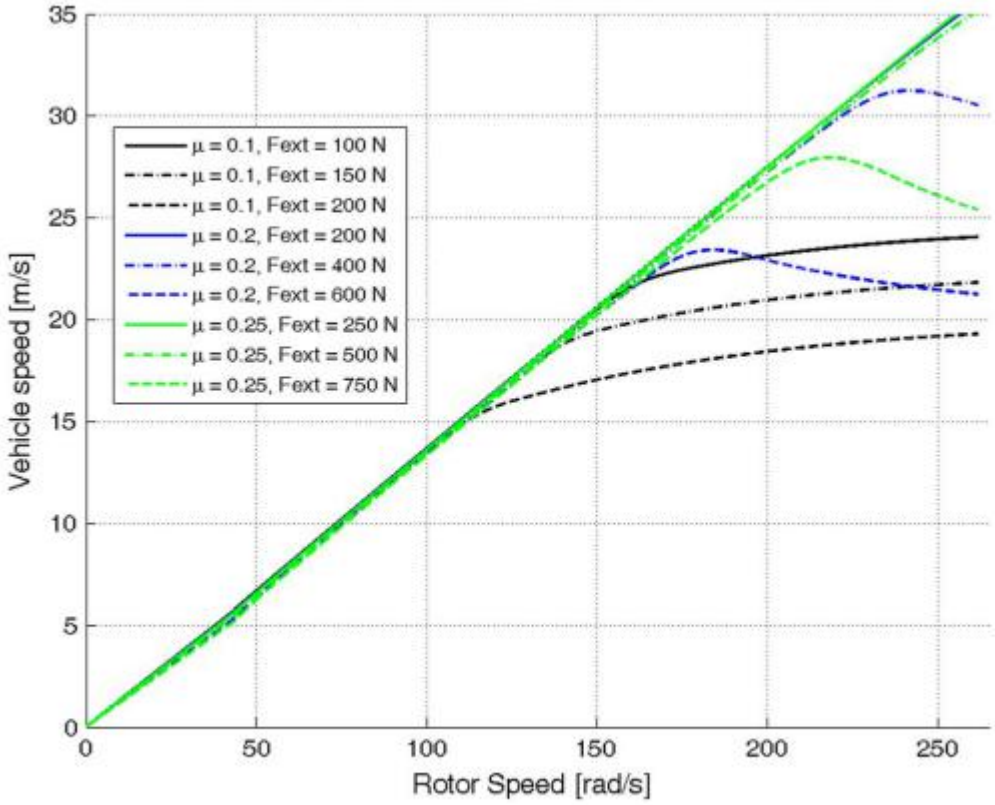

Figure 3.4: Representation of the $g_{\mu i}$ curves, in the (ω, v) plane

Is possible therefore to write:

$$v_x = g_\mu(\omega_l) \tag{3.4.2}$$

$$\frac{dg_\mu(\omega_l)}{d\omega_l} \geq c_g > 0. \tag{3.4.3}$$

By eliminating the slip absence hypothesis imposed in the previous section, the equation [3.1.9] must be appropriately modified to:

$$\lambda_{(\omega,v)_{\mu,i}} = \frac{R_\omega \omega_i - g_\mu(\omega_l)}{g_\mu(\omega_l)}. \tag{3.4.4}$$

From this equation is firmly clear the dependence between the slip value and the road conditions.

3.5 Automatic reference generator

The aim is to replace the proposed control by an automatic speed reference generator taking into account constraints on longitudinal tire slip. In particular, the vehicle speed reference v_x^* will no longer represent a given constant external input but will be allowed to vary in order to guarantee at steady state values of λ_i belonging to the safety region. The key-concept, that is similar to the one qualitatively presented in [29], will rely on the contraction theorem [30].
Let us introduce the connected and compact set $\Lambda_\mu = \left[\lambda_{(\mu_a)}, \lambda_{(\mu_b)}\right] \subset R$ that identifies the set of desired slip values, safe for each external condition situation, unknown by definition. Let us assume that the two in-wheel motors are combined in a single central motor, or that the differential speed reference of the motors ω_d is null (later, this approximation will be removed). The goal is to show that it is possible an automatic change of the motor rotation speed ω^* in order to ensure $\lambda_{(\omega,v)_\mu} \epsilon \Lambda_\mu$.
Then, let us define a connected and compact set for the domain of interest of ω, that is $\Omega = [\omega_m, \omega_M] \subset [0, +\infty)$ with $g_\mu(.) : \Omega \to R(g_\mu)$ and a continuous, strictly increasing and infinitely differentiable function that we call f_o, so that the latter does not depend on μ, $f_o : \Omega \to R(f_o)$.
The idea is to create the f_o function in such a way that all his intersection points with the curves g_{μ_i}, which we will call $P_\mu = (v_p^\mu, \omega_p^\mu)$, satisfy the condition $(\mu \epsilon M) : \lambda_{(\omega,v)_\mu} \epsilon \Lambda_\mu$, in the defined domain. When that this goal is reached, it is possible to guarantee that a control on the motor reference speed is automatically generated, adapting to unknown external conditions while keeping the slip values into a safe range.
The function f_o to be design must have the following properties:

- be strictly increasing $f_o \geq c_o > 0$;
- its slope must be greater than the curves: $g_{\mu_i}(\omega_i, v_i), \max_\Omega\{|\acute{g}_\mu|\} / \min_\Omega\{\acute{f}_o(.)\} \leq \alpha < 1$:
- be defined for all permissible values of $v_i, R(f_o) \supseteq R(g_\mu)$.

Logically, the ultimate goal is to guarantee the vehicle operation at $P_\mu = (v_p, \omega_p)$ without knowing μ_i, (because they are unknown parameters) and only relying on the (ω, v) measurements through an iteration.
However, if we think about the information just presented, by definition $\lambda_{\left(\omega^*, g_\mu(\omega^*)\right)_\mu}$ is continuous function in ω_i, and constant for a linear and increasing value of $g_\mu(\omega)$; indeed $g_\mu(\omega) - \omega \frac{dg_\mu(\omega)}{d\omega} > 0$. So, because of the constraints imposed on f_o , the existence of a single point $P_\mu = (v_p, \omega_p)$ in Ω is guaranteed.

Proff
To prove the above statement we introduce the map:

$$T(.) = f_o^{-1}(g_\mu(.)) \tag{3.5.1}$$

This is well defined because the third property of f_o, guarantees that its codomain is an improper subset of that of $g_\mu, dom(f_o^{-1}) = R(f_o) \supseteq R(g_\mu)$.

The map $T(.)$ is a contraction on Ω; according to the mean value theorem for $(\varepsilon\epsilon(\omega_1, \omega_2))$, we obtain:

$$|T(\omega_1) - T(\omega_2)| = |T(\varepsilon)||\omega_1 - \omega_2|, \tag{3.5.2}$$

with $|T(\varepsilon)| \leq \alpha < 1$.
Thus, by choosing any $\omega^{*0}\epsilon\Omega$, it can be defined the iterative sequence of rotor speed reference values (ω^{*i}) as follows:

$$\omega^{*0}, \omega^{*1} = T(\omega^{*0}), \omega^{*2} = T(\omega^{*1}) = T^2(\omega^{*0}), \ldots. \tag{3.5.3}$$

Now we will show that the sequence generated by the application of $T(.)$ at (ω^{*i}) remains in Ω, and is a Cauchy that converges to a unique $\omega^{*a}\epsilon\Omega$.
In fact, it is possible to write:

$$\begin{aligned} |\omega^{*m+1} - \omega^{*m}| &= T(\omega^{*m}) - T(\omega^{*m-1}) \leq \alpha|\omega^{*m} - \omega^{*m-1}| \\ &= \alpha|T(\omega^{*m-1}) - T(\omega^{*m-2})| \leq \alpha^2|\omega^{*m-1} - \omega^{*m-2}| \ldots \\ \ldots &\leq \alpha^m|\omega^{*1} - \omega^{*0}|, \end{aligned} \tag{3.5.4}$$

while, by the triangle inequality, we have for $n > m$:

$$\begin{aligned} |\omega^{*m+1} - \omega^{*n}| &\leq |\omega^{*m} - \omega^{*m+1}| + \ldots + ||\omega^{*n+1} - \omega^{*n}| \\ &\leq (\alpha^m + \ldots + \alpha^{n-1})|\omega^{*1} - \omega^{*0}| \leq \frac{\alpha_m}{1-\alpha}|\omega^{*1} - \omega^{*0}|. \end{aligned} \tag{3.5.5}$$

Since Ω is closed and complete, we can affirm that (ω^{*i}) converges,
$(\omega^{*i}) \to (\omega^{*\alpha})$. The above equations imply that:

$$|\omega^{*\alpha} - T(\omega^{*\alpha})| \leq |\omega^{*\alpha} - \omega^{*m}| + |\omega^{*m} - T(\omega^{*\alpha})| \leq |\omega^{*\alpha} - \omega^{*m}| + \alpha|\omega^{*m-1} - \omega^{*\alpha}|. \tag{3.5.6}$$

The sum of the right terms can be made arbitrarily small for a big enough m value, then we can thus establish that $|\omega^{*\alpha} - T(\omega^{*\alpha})| = 0$. Using the second property of norms N_2' shown in [30], then $\omega^{*\alpha} = T(\omega^{*\alpha})$. The existence of the point mentioned above has been guaranteed; now it is necessary to prove it is unique; however if we suppose that there are two fixed points of $T(.)$, respectively $\omega^{*\alpha 1}$ and $\omega^{*\alpha 2}$, such that $\omega^{*\alpha 1} = T(\omega^{*\alpha 1})$ e $\omega^{*\alpha 2} = T(\omega^{*\alpha 2})$, we get $|\omega^{*\alpha 1} - \omega^{*\alpha 2}| = |T(\omega^{*\alpha 1}) - T(\omega^{*\alpha 2})| \leq \alpha|\omega^{*\alpha 1} - \omega^{*\alpha 2}|$ and being $\alpha < 1$, the unique possible solution is $\omega^{*\alpha 1} = \omega^{*\alpha 2}$.
The proof just presented is based on the belief that $T(.)$ is a contraction not on the entire space R but merely on the compact set $\Omega \subset R$, i.e. the (ω^{*i}) remains in Ω. This hypothesis can be proven by mathematical induction, using the first and second properties of the f_o function.
Since $g_\mu(l)$ with the $l\epsilon\Omega$ satisfies:

$$f_o(\omega_m) \leq \min_{\Omega} g_\mu(.) \leq g_\mu(l) \leq \max_{\Omega} g_\mu(.) \leq f_o(\omega_M), \tag{3.5.7}$$

then $f_o^{-1}\Big(g_\mu(l)\Big)\epsilon\Omega$.
The point $\omega^{*\alpha}$ is the value ω_p^μ at the intersection point P_μ, which also corresponds v_p^μ.

$$g_\mu(\omega^{*\alpha}) = f_o(\omega^{*\alpha}) = P_\mu(\omega_p^\mu, v_p^\mu). \tag{3.5.8}$$

Figure 3.5 highlights the intersection points of the f_o con $g_{\mu i}$ for $i\epsilon\{1,2,3\}$, each of them defining a single $\omega^{\mu} = \omega^{*\alpha i}$.

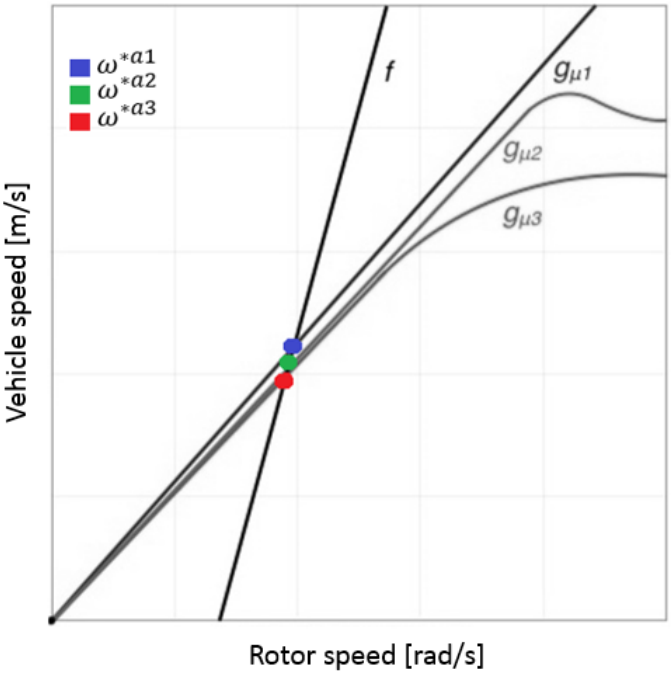

Figure 3.5: Intersection of f_0 with $g_{\mu i}$, for $i\epsilon\{1,2,3\}$

In summary, we proved the existence of the f_0 function and, even if the parameters μ_i are unknown, we can guarantee the convergence of the sequence (ω^{*i}) to $\omega^{*\alpha}$. This sequence is the ω_p^{μ} value at the intersection point f_0 and the $g_{\mu i}$ functions, where by definition the slip λ_i is low, belonging to the set Λ_{μ}.
We are nearly there, our long mathematical journey is almost finished. In the situation of high slip values, on the basis of the knowledge of the measurements will be possible to provide a new value for the motor rotor speed, defined in the point $P_{\mu}(\omega_p^{\mu}, v_p^{\mu})$ and guarantee his achievement thorough an iteration process.
Let us call $\omega_{ref}^{f}(t)$ the speed control of the electric motor, (where f denotes the filtered signal), instead of ω^* (estimated according v^*, set by the driver). In order to obtain a class C^2 signal, based on the motor reference values ω^{*i}, to be provided as input to the speed control $\omega_{ref}^{f}(t)$, then we define positive real values γ_i with $i\epsilon\{1,2,3\}$ such that the dynamics matrix is Hurwitz:

$$\omega_{ref}^{f}(t) = \gamma_1\pi_1 \tag{3.5.9}$$
$$\dot{\pi}_1 = \pi_2 \tag{3.5.10}$$
$$\dot{\pi}_2 = \pi_3 \tag{3.5.11}$$
$$\dot{\pi}_3 = -\gamma_1\pi_1 - \gamma_2\pi_2 - \gamma_3\pi_3 + \omega_{ref}^{f}(t), \tag{3.5.12}$$

where $\omega_{ref}^{f}(t) = \sum_{0}^{+\infty} \chi(t)_{[i_\alpha,(i+1)_\alpha]}\omega^{*i}$, α is a positive constant and $\chi(t)_W$ is a characteristic function of the connected set W.

For each constant input c of the filter, the exponential convergence of π_1 can be tested as in [32], considering the error dynamics of $\left(\frac{\omega^f_{ref}}{\gamma_1} - \frac{c}{\gamma_2\pi_2\pi_3}\right)$. Assuming that the above filter dynamics and the tracking error $(\omega - \omega^f_{ref})$ are fast enough to guarantee the existence of a constant $a > b$, then the approximation:

$$\omega(i\alpha + s) \approx \omega^f_{ref}(i\alpha + s) \quad i = 0, 1, \ldots \tag{3.5.13}$$

is true for every $s\epsilon[b, (i+1)a]$. Finally, we can affirm that the sequence of points (ω^i, v^i) at time instant $t = ia + s$, $i = 0, 1, \ldots$ is equal to $(\omega^{*i}, g_\mu(\omega^{*i}))$.
Therefore the convergence of the sequence (ω^{*i}) to $\omega^{*\alpha}$ guarantees the convergence of ω^f_{ref} to ω^μ. The process described for the generation of the rotor speed ω^f_{ref} through the contraction mapping theorem can be shown in figure 3.6, where the contraction mapping region (ω, v) is shaded in blue, with slip values λ_i not belonging to the Λ_μ. set. The defined safety region is highlighted in green.Through a repeated application of the map $T(.)$ it is possible to guarantee the algorithm convergence from the point $''1''$ to the intersection point $P_\mu(\omega^\mu_p, v^\mu_p)$.

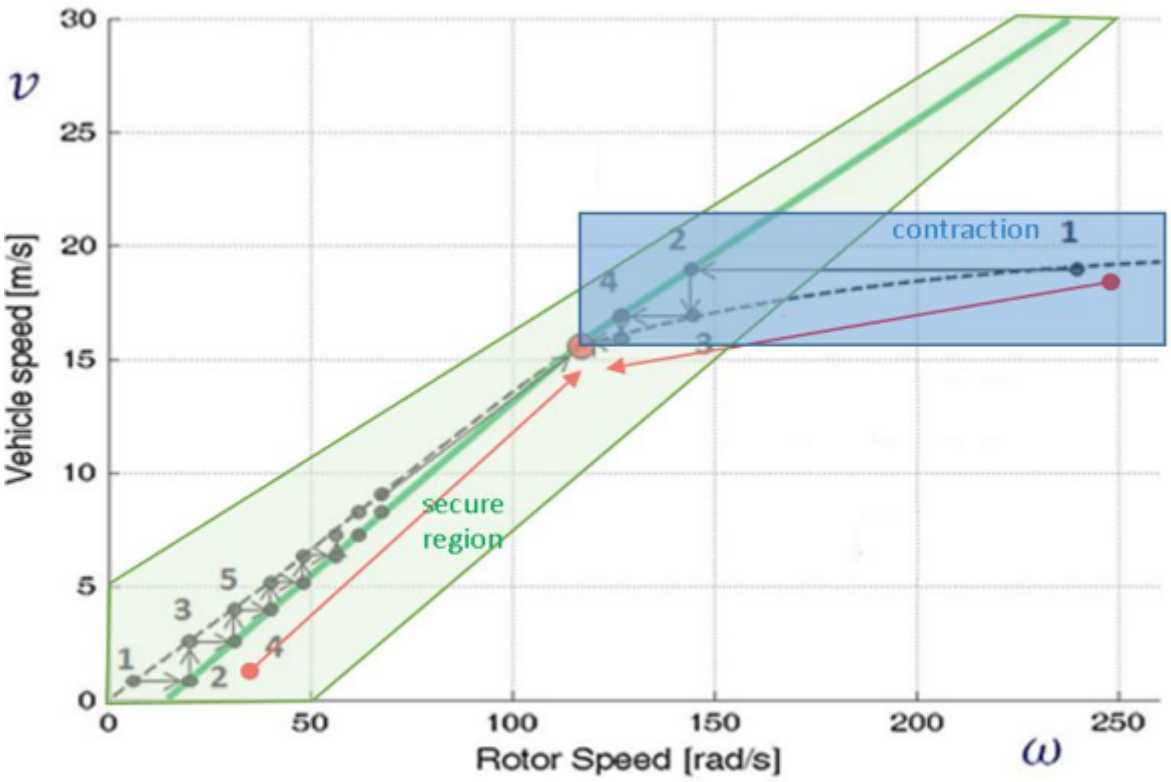

Figure 3.6: Automatic generation of the rotor velocity ω^f_{ref}

3.6 Generalizations for In-Wheel motors

So far has been presented and tested the algorithm to achieve a desired operating point P_μ without knowing the external parameters, considering the hypothesis that two in-wheel motors are combined in a single central motor.
Let us eliminate this restriction and, depending on a given steering angle δ, constrain the differential speed reference ω_d to meet the open-loop kinematic chain:

$$\omega_d^* = \frac{l_\omega r^*}{R_\omega} = \frac{l_\omega \delta v_x^*}{R_\omega (l_f + l_r)} = \frac{l_\omega \delta \omega_l^*}{(l_f + l_r)}. \tag{3.6.1}$$

Remember that the operating condition at steady state (ω, v_x) defines a specific curve $g_\mu(.)$ in the plane (ω, v_x). At the same time, these curves (shown in figure 3.4), intersect the function f_o, as in figure 3.5.
Considering the curves performances at the operative points and the very fast response of the motors controls, we define, as previously, a sequence of references (ω_l, ω_d) which converges to a single operating point P_μ.

In fact, it is possible to create a function $f_{\acute{o}}$ that implies $\omega_l^* = f_{\acute{o}}^{(-1)}(v_x^*)$; however the rotation speed will not still be that of the rotor, but in accordance with the equations [3.3(5-6)] ω_l, as well as ω_d, will depend on the rotation sped of the rear wheels ω_{rl}, ω_{rr} but this counts for little.
Defining the relationship between ω_l^* and ω_d^* at every instant (t) and applying the contraction theorem, as in section [3.5], it is plausible to affirm that λ_i values belonging to the safety region Λ_μ, can be guaranteed.

CHAPTER 4

Experimental set-up

This chapter describes the proposed set-up for the experimental verification and validation of the control system. The first part describes in detail the model car in scale used, its mechanical modifications, actuators and sensors; then presents the selected algorithms for steering control, rear wheels and motors angular speed control. Finally, it explains the implementation of the Kalman filter for the compensation of the measurements errors.

4.1 Vehicle model

The model car used for the experimental tests was the S10 Blast TC2 of the German producer LRP, shown in figure 4.1. It is a 1:10 scale reproduction of a stock car and is designed to be used also in professional competitions between radio controlled (RC) cars.

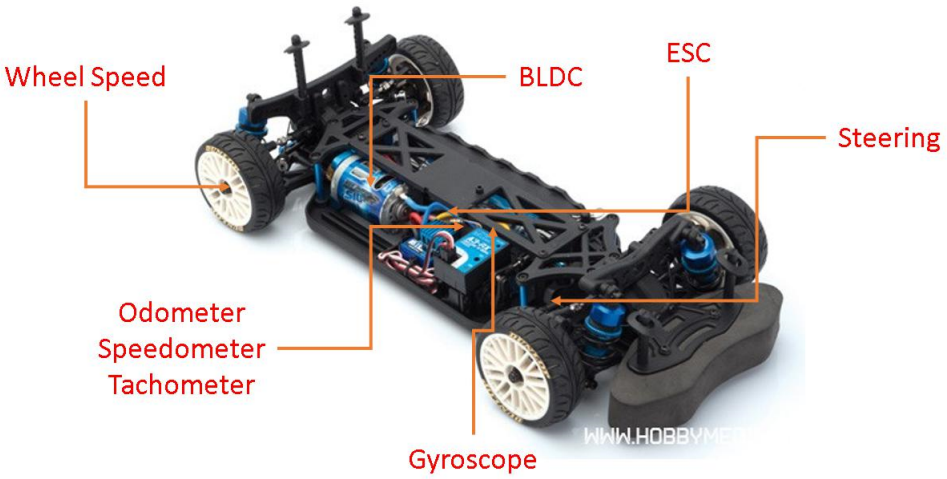

Figure 4.1: Vehicle model S10 BLAST TC2 in scale 1:10

The model car is characterized by an extremely complex and realistic mechanics: it is equipped with four wheel drive (FWD), hydraulic oil suspension, stabilizer bars for all wheels, ball bearings on all supports and two metallic differentials. The proposed model car is not suitable for experimental tests on controls based on electric motor vehicles powered by two in-wheel motors. Therefore, it was necessary to modify the experimental set-up. First, the FWD traction, i.e. the distribution of the vehicle's driving torque on all four wheels, must be eliminated, since the rear wheels must be independent from the front wheels. In addition, it was necessary to dismount the rear differential, which guaranteed an equal distribution of the driving torque between the two drive wheels, because the wheels must be free to rotate at different angular speeds. Finally, it was necessary to provide enough space to lodge the modules required by the experimental set-up, such as sensors, actuators and development board.

4.1.1 Mechanical modifications

The aim was to adapt the mechanics to the specific project requirements without compromising stability and, above all, the integrity of the system. First, everything that was not strictly necessary or was too cumbersome was disassembled: the platform, the differential and the rear suspension were removed. As the FWD traction mechanism prevented independent wheel control, it was removed; at this point, regarding the transmission, the crankshaft was useless, but still necessary to measure the vehicle's speed. Then it was cut into two equal sections and one of the two halves was secured to the frame and connected to a Rotary Encoder (RE), in order to obtain the odometrical measurements of the vehicle.

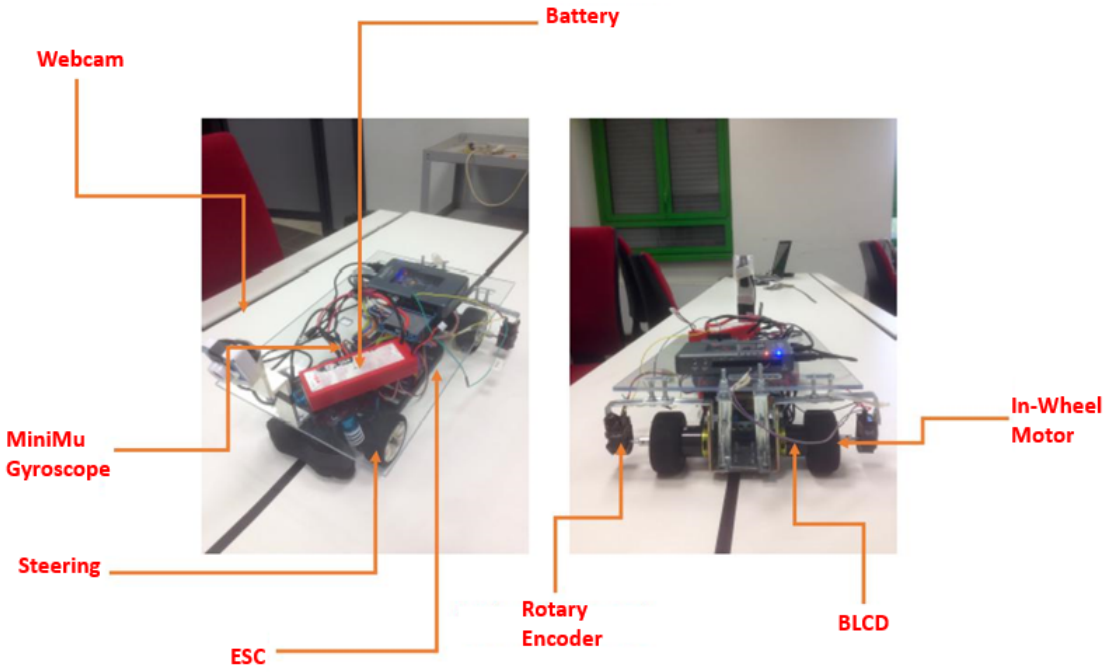

Figure 4.2: Modified vehicle model in scale 1:10

For In-Wheel propulsion, the wheels were fastened directly to the motors, using bolts. The biggest challenge was to design the compartment to house the wheels, the motors and their RE. Different solutions were evaluated, some very simple others that implied the use of precision mechanics tools. At the end, a compromise was made: two metal L-shaped brackets were used, (to create a sort of U) on which the motors and wheels were fixed. Both sides of this support have been equipped with aluminium "extensions" whose role was to support the RE used to measure the motors rotor speed. The support was fixed on the chassis, replacing the rear floor. This step was done with a lot of caution and precision: a badly fixed or mounted screw causing a wrong angle between the rear and the front wheels could have caused the vehicle imprecise trajectory and a decrease the stability of the system. As can be observed in figure 4.2, the modified model car is extremely different from the original one, provided by the manufacturer. Hardware and mounted sensors have increased its weight (decreasing its performance in terms of speed), but without compromising its stability and integrity.

4.2 Actuators

Two types of actuators were: two BLDC sensorless motors with Electronic system control (ESC) and one servomotor. Both devices are controlled in Pulse Width Modulation (PWM). Typically, in a RC model the PWM signal is generated by a radio controler-radio transmitter (RC-RT) system with pulse rate at 50 Hz and width between 1 ms and 2 ms with a neutral point at 1.5 ms. In the proposed set-up, the servomotor maintained the same communication protocol, while the DCBM motors had an increase of the pulse rate up to 200 Hz. For BLDC motors, a proportional integral control based on fuzzy logic was implemented to ensure that the rotor speed adjustments were quickly completed; for the servomotor an autonomous driving algorithm has been chosen.

Figure 4.3: Actuators mounted on the vehicle

4.2.1 DC-Brushless sensorless motors

The DC-Brushless motor (BLDC) is formed by a stationary component, the stator, and a rotating component, called the rotor. The rotor consists in permanent magnets, while the stator is made up of coils capable of developing a magnetic field. The interaction between the magnetic field and the permanent magnets allows the rotor to rotate. The BLDC motor has the following advantages: quick response and easy control, as commutator system uses Hall Effect sensors instead of mechanical brushes, low noise and no mechanical losses. This type of engine is widely used in many systems, such as in compact disc control drivers.
For the experimental set-up were used two 3-phased sensorless BLDC "TRX-AIR.25" motors, able to deliver a power of 770W. An ESC Hobbywing Xerun 120A drives the motors. This motor category eliminates the Hall Effect sensor, using unexcited spires as a position sensor for the commuting. A typical method for locating the rotor position is to identify an electromotive force in the coils, as illustrated in [17]. A different procedure, described in [18], is based on the on/off state of the H-bridge to determine the switching moment.
The resulting open loop control is shown in figure 4.4.

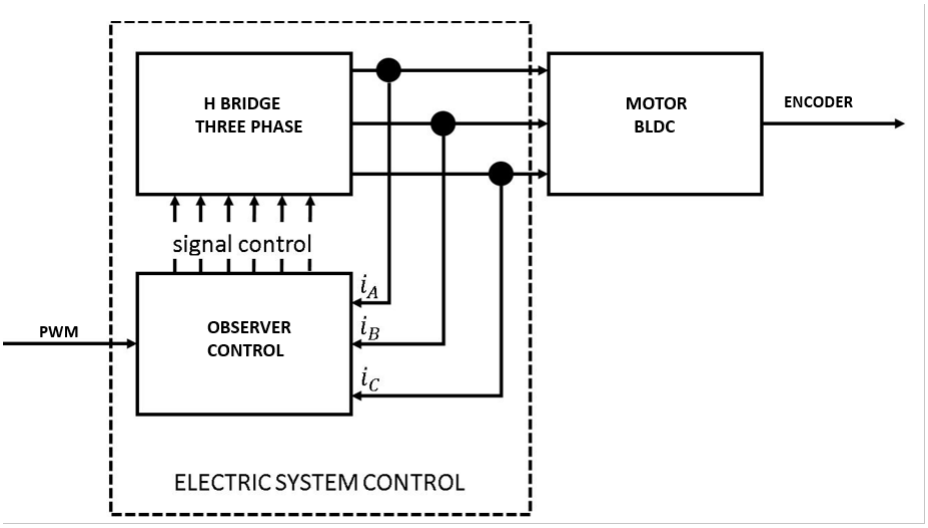

Figure 4.4: Block diagram of the internal BLDC Sensorless control

4.2.2 DC servomotor

The second type of actuator was a servomotor, used to steer the front wheels. A generic servomotor looks as a small plastic container with a pivot that can rotated from 0 and 180 degrees while stably maintains the reached position. A DC motor is used to achieve the pivot rotation and a demultiplying mechanism can modify the torque during rotation. An internal control circuit carries out the motor rotation; this circuit is able to detect the rotation angle reached by the pivot through a resistive potentiometer and to stop the motor at the desired point.

4.3 Sensors

The model was equipped with sensors capable of providing the necessary measurements to get a proper control function. Precisely, the design specifications require that the vehicle longitudinal speed, both BLDC rotor speeds and the vehicle yaw rate are all known values. The measurements were performed using two types of sensors: a Rotary Encoder and a Gyroscope.

4.3.1 Rotary encoder

An angular position transducer is an electromechanical device that converts an angular position or motion to a digital code. There are several types of rotary encoders; for the this project we used the particular type that converts the angular position of its rotating axle into short electrical impulses that need to be elaborated by a signal analysis circuit as digital numeric signals.
In its simplest form, two parts can be distinguished: the body, which constitutes the static part and contains the electronic components (sensors, circuits etc.), and the rotor that constitutes the rotating part, which normally ends with a shaft to be connected to the axle where the reading is performed. The electrical output signals transmit information about the relative position or displacement of the rotor from the body. The encoders are made based on four different principles of transduction: Capacitive/Inductive encoders, Magnetic Encoders, Potentiometer encoders and Optical Encoders. In the last, optical sensor (photoresistors or photodiodes) read a matrix of transparent (holes) and opaque areas, printed on the rotor. In a similar way than in the capacitive encoders, this matrix made with alternating areas, allows to codify a rotor sector equivalent to its angular resolution. In this project were used three Optical encoders from Avago Technologies, shown in figure 4.5

Figure 4.5: Rotary encoder '' Avago Technologies ''

The encoder used is characterized by the presence of a second photodiode, positioned 90 degrees out of phase from the other and connected to an additional channel. This technique, called quadrature, has two significant advantages (figure 4.6), allowing to quadruplicate the transducer digital resolution, because as they are 90 degrees out of phase between each other, the possible digital states are four instead of two. Each sensor behaves like a bit and the direction of rotation can be detected, because with a given reference (as in the figure), first channel A will lead channel B; then, when rotates in the opposite direction, channel B will lead channel A.

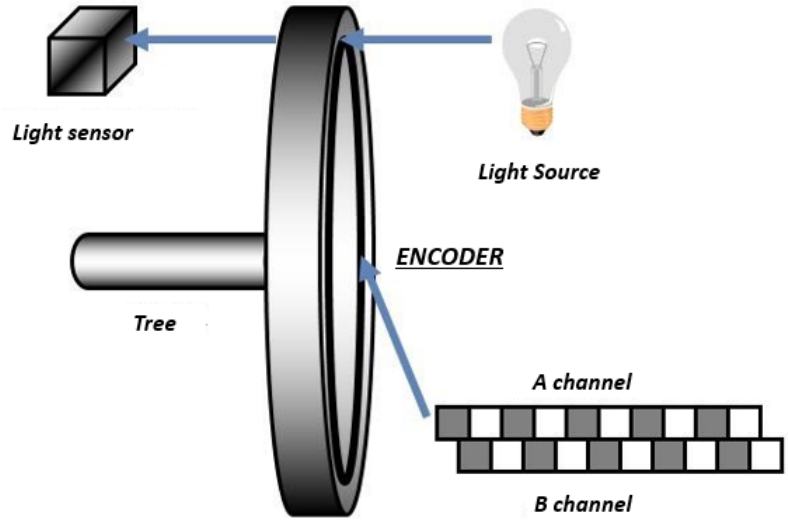

Figure 4.6: Working principle of a quadrature rotary encoder

4.3.2 Gyroscope

In general, a gyroscope is defined as a rotating physical device that due to the law of conservation of angular momentum, maintains its spin axis oriented to a fixed direction. In recent years, MEMS gyroscopes have found extensive use. Most of the gyroscopes on the market are vibrating gyroscopes, exploiting the inertia accelerations arising from the motion of the sensor compared to a non-inertial reference system (in this case, the acceleration of Coriolis). These systems use highly sensitive piezoelectric crystal sensors. In this project was chosen a L3GD20H gyroscope produced by STMicroelectronics, which also has an accelerometer and a compass, mounted on a Pololu MinIMU9 chip, shown in figure 4.7.
The L3GD20H is a low-power three-axis angular rate sensor. It includes a sensing element and an I2C/SPI interface able to communicate to the external world. It is possible to program the device to change the resolution scale and to filter the data. By I2C, the Output Data Rate was set to 200 Hz, and a cut-off was set to 100 Hz.

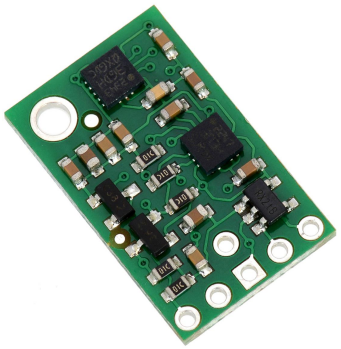

Figure 4.7: Pololu MinIMU-9 where is mounted the gyroscope L3GD20H and the accelerometer/compass LSM303D

4.3.3 Webcam

As was explained before, to demonstrate the validity of the proposed control, an autonomous driving algorithm is applied in order to allow the vehicle to travel autonomously following a pre-set path. To guarantee the recognition of the path it was necessary to mount a webcam on the vehicle, connected with the development board using a USB protocol. Figure 4.8 shows this sensor and its positioning.

Figure 4.8: Webcam

4.4 Implementation of the algorithm on the vehicle

Once the vehicle modifications were carried out, it was necessary to use a programmable hardware platform capable to get real time inputs from the mounted sensors, process them and deliver the outputs according to the control model formulated. The myRio device from National Instruments is able to perform all these functions in a remarkable way. By using it in combination with the LabVIEW program, not only was possible to implement the control presented in the third chapter but even an autonomous driving algorithm. In the following pages there is a detailed description of the development board and the method implemented for its programming. Subsequently, are shown the practical architecture of the autonomous driving algorithm and the Fuzzy Logic Proportional-Integral Control used to regulate the rotor speed of the two motors.

4.4.1 Development board

The myRio is an embedded device (figure 4.9), with configurable inputs and outputs that make it extremely powerful and versatile; is perfect to be used in control systems, robotics or mechatronic projects and is relatively easy to configure and program using the LabVIEW (Laboratory Virtual Instrumentation Engineering Workbench) from NI, or other "classic" programming languages such as C or C++. The reason for this versatility is easy to understand by reading its technical specifications provided by NI ([40]); the myRio combines a dual-core ARM Cortex-A9 processor (allowing the input and output data processing in real-time) with a Xilinx FPGA Zynq-7010.

Figure 4.9: NI myRIO

The device is able to interface with the outside world thanks to both analogic and digital inputs and outputs grouped into three ports.

Two of these are MXP interface, while the third is a MSP interfase (figure 4.10).
The NI myRio also has a 256 MB non-volatile memory, a 512 MB DDR3 RAM, an audio output, configurable buttons, LEDs and an accelerometer; it can be controlled by the user via USB 2.0 ports or via Wi-Fi. Additionally, it has a Xilinx zynq-7010 whose block diagram is shown in figure 4.10.

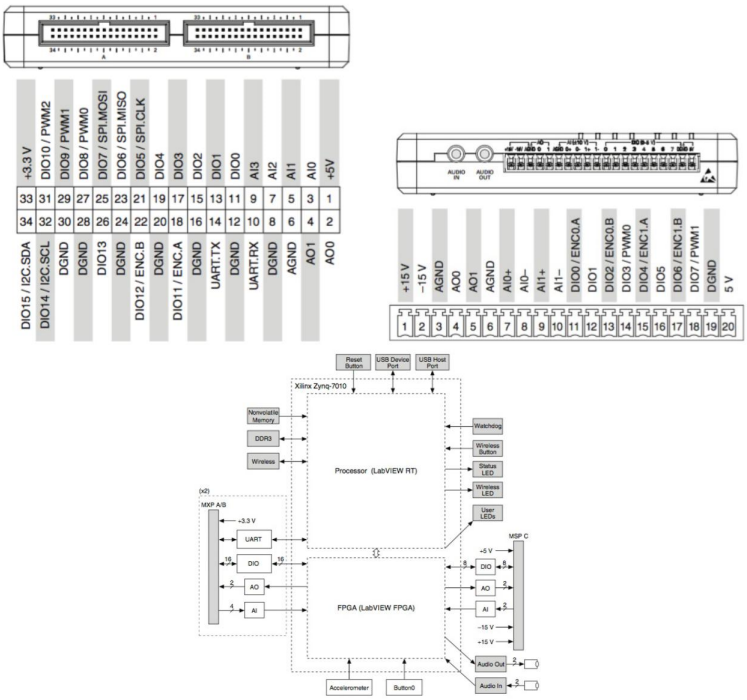

Figure 4.10: Interface mxp, interface msp and block diagram Xilinx Zynq-7010

4.4.2 Programming using LabVIEW

LabVIEW, a system-design platform and development environment for a visual programming language from National Instruments, was used for programming the myRio Development Boar.
The programming language used by LabVIEW is different from the traditional languages because its syntax is not written but graphic (figure 4.11). The definition of data structures and algorithms is done with icons and other graphical objects, each of which encapsulates different functions, connecting wires, so as to form a flowchart-like data flow. This type of language is called data flow programming because the execution sequence is defined and represented by the data flow itself through the unidirectional wires that connect the functional blocks. The execution of a program follows some simple logic rules: each block is executed as soon as all its input data become available. If the programmer does not specify different priorities between them, the blocks are run from top to bottom and from left to right; if there are one or more wires that are not linked to blocks or constants, the program is not executable. Because the data can also flow in parallel, via blocks and non-consecutive wires, the language can automatically create multi threading without the need for explicit management by the programmer.
In general, using LabVIEW is possible to simulate dynamic systems, acquire data,

analyse analogic and digital data, perform very complicated calculations with input data, and perform tools and equipment controls.
In essence, therefore, with LabVIEW you can bring information from the real outside world to the operator's computer, process this data and send it back to control a particular instrument. Exactly what we need.

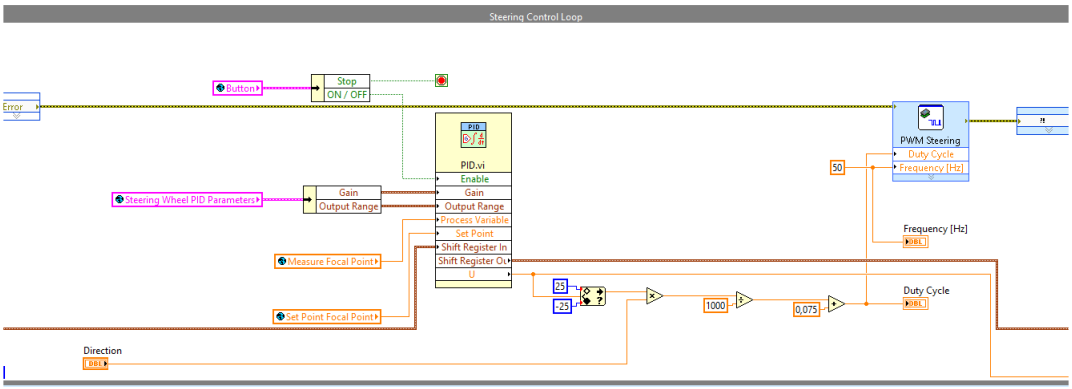

Figure 4.11: Steering wheel loop control block diagram on LabVIEW

4.4.3 Autonomous driving algorithm

Let us review what we have done so far. Summarizing, the vehicle was prepared to meet the In-Wheel technology architecture, the actuators and the development board needed to get the input data were mounted, and finally it was explained how the data were analysed and processed using LabVIEW, producing their respective output. At this point, we were ready to implement the "Cruise Control under Slip Constraints" and to verify its function and performance. In practice, the vehicle had to travel a path and, at the same time, its longitudinal speed or yaw rate had to be controlled only by the implemented algorithm. It was illogical to use a radio control – radio transmitter system, then, as previously stated, an autonomous driving algorithm was implemented. First, it was necessary to identify a particular path for the algorithm to function properly. The chosen path was marked by placing a red ribbon on the road surface. The external image was then acquired through the vehicle webcam. The identification algorithm called "Pattern Matching Recognition" has the task of identifying the line or pattern and calculating its position relative to the vehicle's barycentre. Then, another control, defined ''Geometric Path Tracking'', calculates the front wheels steering angle δ^* necessary to follow the fixed route.

4.4.4 Pattern Matching Recognition

The path image is acquired by the webcam, then filtered and broken down to three primary colours: red, green, and blue. Each colour is encoded using a digital system and has assigned a corresponding Boolean logical value. Specifically, the red colour correspond to the $true$, the others to the $false$. This implementation originates the $R\overline{GB}$. In practice, each pixel is represented as binary values and using a polynomial approximation based on Doolittle decomposition and on least squares, the presence of red is enhanced, together with the complete absence of blue and green. In figure 4.12, on the left is shown the image of a path captured by the webcam; on the right is visible the matrix of the image already processed and the resulting combination $R\overline{GB}$.

Figure 4.12: $R\overline{GB}$ combination

Although the path is now recognised, the incoming information is not sufficient to identify the variable position of the point to follow, called (g_x, g_y). Often, the image captured have noise, and may appear $true$ values in regions different from the highlighted path. To overcome this problem, an average pixel width L is defined, which identifies the $R\overline{GB}$ combination on each line and a search algorithm is implemented. This control will guarantee the correct red colour detection and the point (g_x, g_y) will be the midpoint of L width. In figure 4.13, the pattern search is highlighted within a row of pixels.

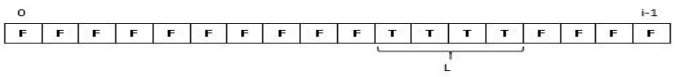

Figure 4.13: Pattern research in a string of pixels

4.4.5 Geometric Path Tracking

The path was fixed and identified; then, it is necessary that the vehicle follows it. A path-tracking algorithm was used to achieve this goal.
Various automatic Path tracking techniques are listed in [22]; however, for this study case one of the most popular technique was chosen, called Pure Pursuit, belonging to the category of Geometric Path Tracking. This category uses the geometric relationships between vehicle and path to determine the control law.
Based on the desired path and the real path followed by the car in absence of trajectory changes, the error between the measured and the estimated curvature is measured; this is called Tracking error. Then, this Tracking error is reduced by changing the steering angle δ. In particular, the Pure Pursuit technique defines the curvature coefficient of the model car using the kinematic model of the bicycle,

$$r^* = \frac{1}{L}\delta v^*, \tag{4.4.1}$$

where L is the distance between front axle and rear axle and δ is the steering angle. As shown in figure 4.14, the relationship between the steering angle and radius of curvature can be written as:

$$\tan(\delta) = \frac{L}{R}, \tag{4.4.2}$$

where δ is the steering angle of the front wheels and R is the radius of the circular arc traced by the rear wheels, with the given steering angle.

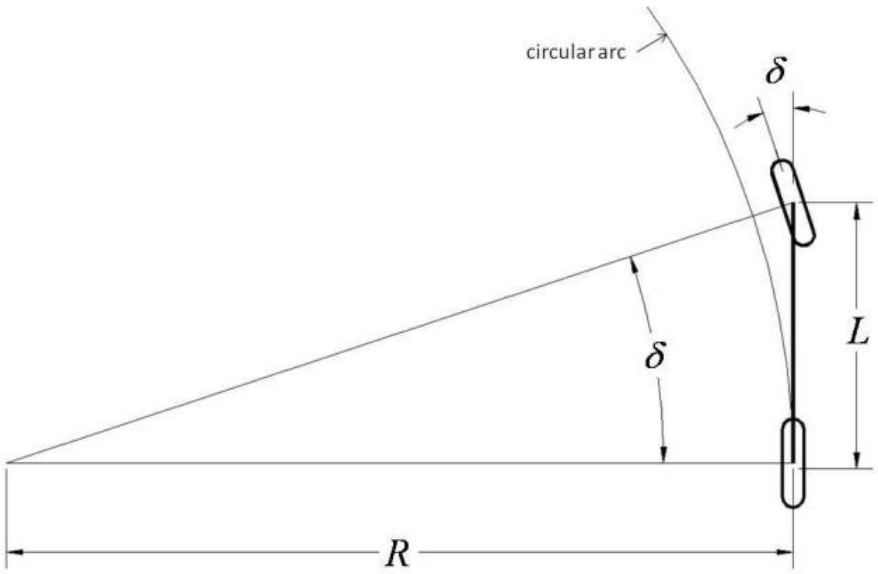

Figure 4.14: Kinematic model of a bicycle during a bending manoeuvre

Setting a desired point of arrival (g_x, g_y), identified by the Pattern Matching Recognition algorithm, it is possible to determine the necessary value of the steering angle δ^*, using a pure geometrical relation.

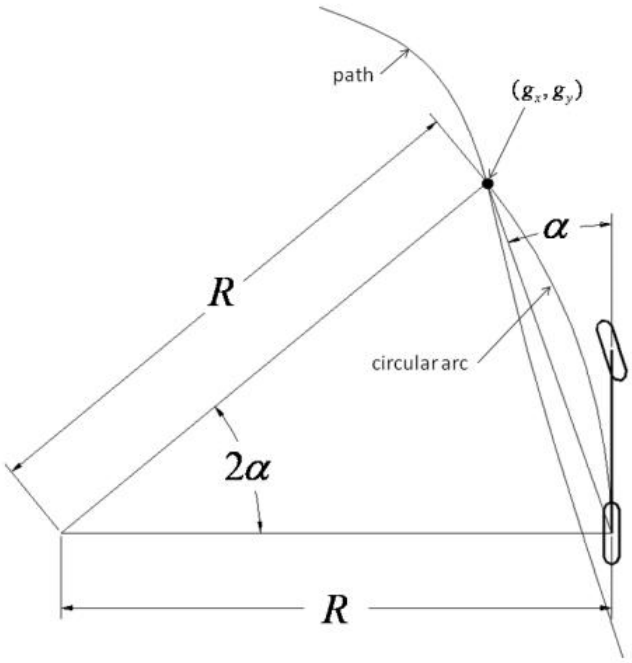

Figure 4.15: Geometric relations used for the calculation of the steering wheel angle

With reference to figure 4.15, it can be written:

$$\frac{L}{\sin(2\alpha)} = \frac{R}{\sin(\frac{\pi}{2} - \alpha)} \tag{4.4.3}$$

$$\frac{L}{2\sin(\alpha)\cos(\alpha)} = \frac{R}{\cos(\alpha)} \tag{4.4.4}$$

$$\frac{L}{\sin(\alpha)} = 2R \tag{4.4.5}$$

$$R = \frac{1}{k} \tag{4.4.6}$$

$$k = \frac{2\sin(\alpha)}{R}, \tag{4.4.7}$$

where k is the curvature of the circular arc. Then, establishing the relationship between L and $\sin(\alpha)$ with the values of the desired point (g_x, g_y):

$$\delta^* = \arctan\left(\frac{2g_x L}{g_x^2 + g_y^2}\right), \tag{4.4.8}$$

where the steering angle depends of the measurement of the desired point of arrival and the length of the vehicle.
Here it is important to note that, according to the above equations, is possible to use a reverse procedure and determine the vehicle point of arrival, if its trajectory is not

modified, i.e. for a fixed steering angle δ_0; as described as follow:

$$k = \frac{\tan(\delta_0)}{L} \tag{4.4.9}$$

$$g_{x0} = R - \text{sgn}(k)\sqrt{R^2 - g_{y0}^2}, \tag{4.4.10}$$

where g_{y0} is fixed.
We are almost at the end. The point of arrival of the vehicle has been identified in the absence of external modification, and was called $P_0 = (g_{x0}, g_{y0})$; the desired point of arrival $P_d = (g_x, g_y)$ is identified through the Pattern Matching Recognition (Block diagram in figure 4.16).
In parallel, we calculate the desired steering angle δ_{FF} and define the error of tracking as the distance between the two points, $e = g_x - g_{x0}$;as well as its maximum threshold value. If the error is smaller than the fixed value, the steering angle will be defined by open loop using equation [4.4.8]; if the error is bigger, we implement an action in feedback by a simple proportional integral control over the error, such that:

$$\delta(e) = \begin{cases} \delta_{FF} & if \quad |e| < e_{max} \\ \delta_{FF} + K_i \int e(\tau)d\tau = \delta_{FF} + \delta_P & if \quad |e| \geq e_{max}. \end{cases} \tag{4.4.11}$$

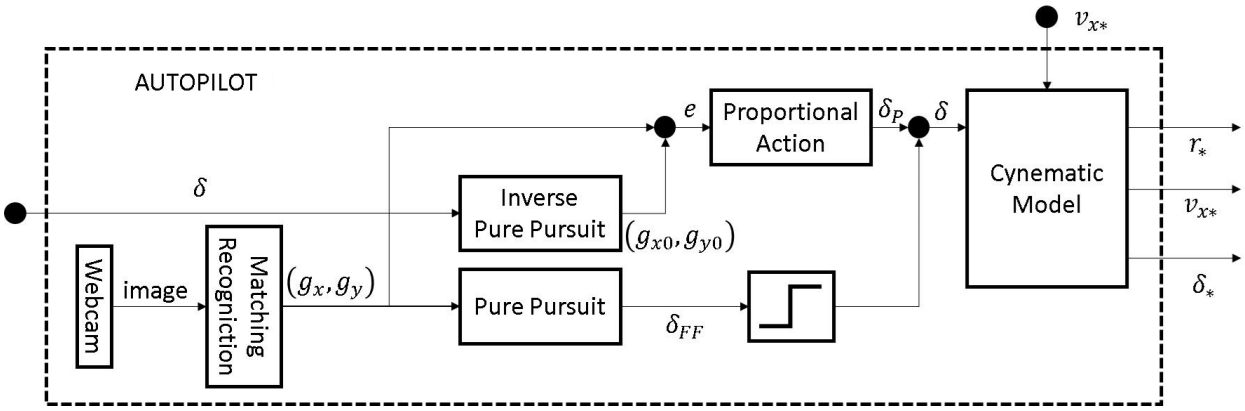

Figure 4.16: Block diagram autopilot

The double control action in open loop and closed loop allows gentle corrections of the steering angle with a constant radius of curvature, as well as other rapid corrections in the case of abrupt changes in the set path curvature.
Note also that if the steering angle δ_0 is zero, then the radius of curvature is infinite. Although the result is mathematically right, because in this situation the curved trajectory degenerates in a rectilinear trajectory, from a practical point of view, it is useful to avoid dividing by zero when using $R = \frac{1}{k+\epsilon}$, with ϵ a positive small constant ϵ.

4.4.6 Fuzzy logic proportional integral control

The last missing piece of the puzzle, also fundamental for the implementation of the proposed algorithm, is the rotor speed control for two in-wheels motors. Their dynamic characteristics are similar to that of a DC permanent magnet motor. The equations that describe its operation are [19]:

$$v_{app} = L\frac{di(t)}{dt} + Ri(t) + v_{emf}(t) \tag{4.4.12}$$

$$v_{emf}(t) = k_b\omega(t) \tag{4.4.13}$$

$$T(t) = k_t i(t) \tag{4.4.14}$$

$$T(t) = J\frac{d\omega(t)}{dt} + D\omega(T), \tag{4.4.15}$$

where $v_{app}(t)$ is the applied voltage, $\omega(t)$ is the motor speed, L is the stator inductance, $i(t)$ is the circuit current, R is the stator resistance, $v_{emf}(t)$ is the electric driving force, $T(t)$ is the engine load torque, D is the viscosity coefficient, J is the inertia moment, k_t is the engine torque costant, and k_b is the constant of the electromotive force. From this equations and depending on the rotor speed of the motor, two transfer functions are obtained:

$$\frac{\omega(s)}{v_{app}(s)} = \begin{cases} \frac{k_t}{(Ls+R)(Js+D)} & if \quad |v_{emf}| \approx 0 \\ \frac{k_t}{(Ls+r)(Js+D)+k_t k_b} & if \quad |v_{emf}| \gg 0, \end{cases} \tag{4.4.16}$$

both stable (minimum phase condition) and therefore controllable by a simple Proportional Integral control. However, the resistance of the stator R and the viscosity coefficient D are usually small and negligible, so the first function, which describes the motor dynamics in the moment of the first detachment, when starting the car, is characterized by one pole at the origin and one real stable pole; the second transfer function, which describes the dynamics within the normal operational region of interest, is characterized by two real stable poles.
The different dynamic performance of the motor brings some technical problems in the case of the implementation of a simple proportional integral control. The use of high gains produces over elongations during the first detachment phase, while the low gains eliminate the over elongations but introduce many transients in the operational region; i.e. making too long the time of adjustment of the motor rotor speed. To solve this problem, it was designed a Fuzzy logic proportional integral derivative control. Examples of this type of approach can be found in [20]. This type of control algorithm, through the implementation of a vehicle with different states, capable of detecting four qualitative states, allows to modify the control gains while maintaining low the over elongations during the first detachment and fast transients in the operational region.
The qualitative states implemented, shown in figure 4.17, are as follows:

- *Friction*: starting of the engine until a percentage ϵ^* of the reference speed is reached. In this state gains are kept low to ensure low over elongations, in other words a careful start;
- *Throttle*: the motor has reached the percentage ϵ^* of the reference speed. In this state a proportional integral derivative control with higher gains is operated to decrease the transients and the error at steady state;

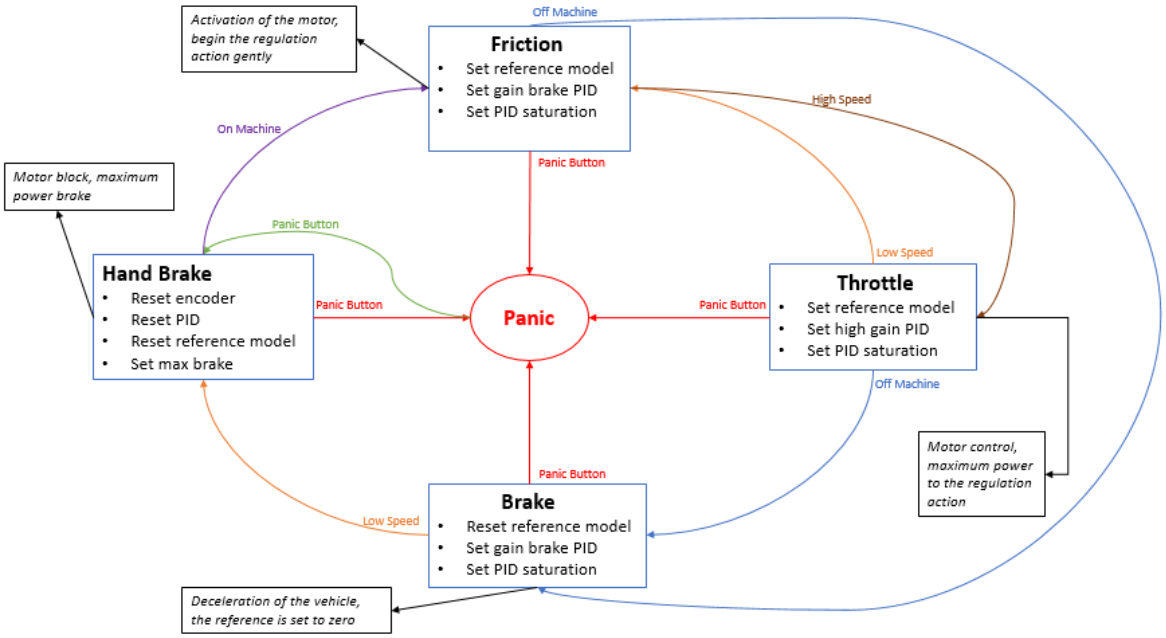

Figure 4.17: Block diagram fuzzy proportional integral control

- *Brake*: engine braking state. The speed reference is brought to zero;
- *Panic*: emergency state, control shut-down;
- *HandBrake*: controls reset state, with pulse width modulation input set in order to get the maximum braking possible.

The Proportional Integral control implemented, as in [25], also provides an anti-windup action. Most control systems are designed using linear theory, but it is often necessary to consider the non-linearity of the model as well. The main factor that determines the non-linearity of the system is the saturation of the actuators. Saturation phenomena, if neglected during the project phase, can lead to closed loop instability. The anti-windup technique allows blocking the definite integral action if there is a saturation phenomenon. The following are the discrete time equations that describe the operation:

$$E[k] = y[k] - r[k] \tag{4.4.17}$$
$$P[K] = K_p E[k] \tag{4.4.18}$$
$$V[k] = P[k] + I[k] \tag{4.4.19}$$
$$U[k] = sat(V[k]) \tag{4.4.20}$$
$$I[k+1] = I[k] + K_i Ek][k] + K_a(U[K] - V[k]), \tag{4.4.21}$$

with $y[k]$ the measurement variable of the process, $r[k]$ the reference, $U[k]$ control chosen, $P[k]$ the proportional action, $I[k]$ the integral action and K_p, K_a, K_i control gains.

4.5 Measurements

At the engineering level, the physical/mathematical models are a powerful tool with the main purpose to describe the object that you want to make and control. The model, in all its forms, is a representation of the physical reality.
In order to improve the output from the rotary encoder and the gyroscope, the measuring system was modelled using Newton's Law:

$$F = ma. \tag{4.5.1}$$

By applying the latter on a single point and differentiating it, the following state estimation was obtained:

$$\begin{bmatrix} \hat{\dot{x}}_1 \\ \hat{\dot{x}}_2 \\ \hat{\dot{x}}_3 \end{bmatrix} = \begin{bmatrix} 0 & 1 & 0 \\ 0 & 0 & 1 \\ 0 & 0 & 0 \end{bmatrix} \begin{bmatrix} \hat{x}_1 \\ \hat{x}_2 \\ \hat{x}_3 \end{bmatrix} + \begin{bmatrix} 1 & 0 & 0 \\ 0 & 1 & 0 \\ 0 & 0 & 1 \end{bmatrix} v \tag{4.5.2}$$

$$\hat{y} = \begin{bmatrix} 1 \\ 0 \\ 0 \end{bmatrix} \hat{x} + \begin{bmatrix} 1 \\ 0 \\ 0 \end{bmatrix} w, \tag{4.5.3}$$

where $[\hat{x}_1, \hat{x}_2, \hat{x}_3]$ represent, respectively, the estimation of the value measured by the particular sensor and its first and second derivatives, $\hat{y}$ is the system estimation, v and w are the measurement errors. In compact form, denoting the model matrices as A, B, C, D the equations characterizing the state and the output become:

$$\hat{\dot{x}} = A\hat{x} + Bv \tag{4.5.4}$$

$$\hat{y} = C\hat{x} + Dw. \tag{4.5.5}$$

From the above equations, it is possible to understand that all measurements are subject to an error, i.e. providing a different result from the real values. This phenomenon is due to the presence, in the model, of measurement errors v and w, called respectively:

- systematic measurement errors: they directly influence the state and are originated from the approximations assumed during model designing phase, or by a wrong calibration of the measuring instrument;
- random measurement errors: they act directly on the output and overlap with the useful signal (ideal measurement).

However, systematic measurement errors can be removed, for example through instrument or sensor calibration processes, while random errors are causal variables (statistical) due to physical uncertainties of the system itself; they cannot be eliminated but compensate. There are two available information to reconstruct the real dynamic state of the system and, in that way, to decrease the noise:

- the mathematical model previously defined;
- measurements made by the sensors, reporting the system value outputs.

Let us suppose that model and the real state system are both excited by the same impulse $u(t)$, as shown in figure 4.18.

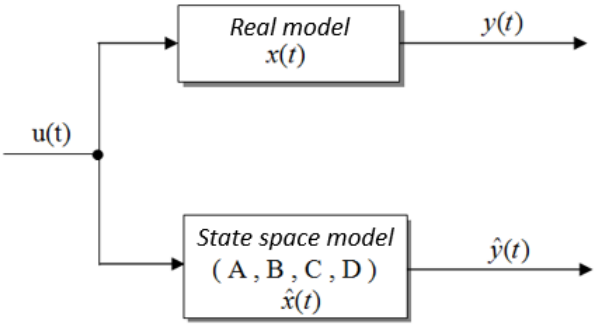

Figure 4.18: State space model and real model excited by the same input $u(t)$

Giving similar stimulating inputs to the real system and to the mathematical model, the outputs should be the same. Unfortunately, this does not happen, because the internal state of the real system at the beginning of the observation and before that moment is unknown. Let us take a step forward, and consider the difference between the two outputs, calling innovation $e(t)$. this difference. If the prediction defined by the model is correct then the error $e(t)$, should be:

- nearly equal to zero: the real value and the estimation values are very similar;
- zero-mean: if $y(t)$ and the estimation $\hat{y}(t)$ differed by a constant value, then it would mean that the model was incorrectly defined because the constant could be predicted and inserted into the equations of the model;
- white: is a statistical characteristic, which implies that between the error $e(t)$ at time (t) and the error $e(t+dt)$ at time $(t+dt)$ there must be no relationship, i.e. they must be independent of each other. If not, it would mean that there is a rule that allows to estimate part of $e(t+dt)$ from the value of $e(t)$ using the same rule. This implies, once again, that there are relationships between signals, but those are defined in the model.

The characteristics listed above are typical of a Gaussian noise.
Finally, let use the error $e(t)$ itself.
As shown in figure 4.19, a gain L value is introduced and through a feedback action "we improve" the estimation state. This, in the situation of a linear and observable system, and with Gaussian noises, can be calculated through the filter of Kalman.

4.5.1 Kalman filter

The Kalman filter allows to build an observer that provides the best estimation of the state, balancing the information from the model and the information from the

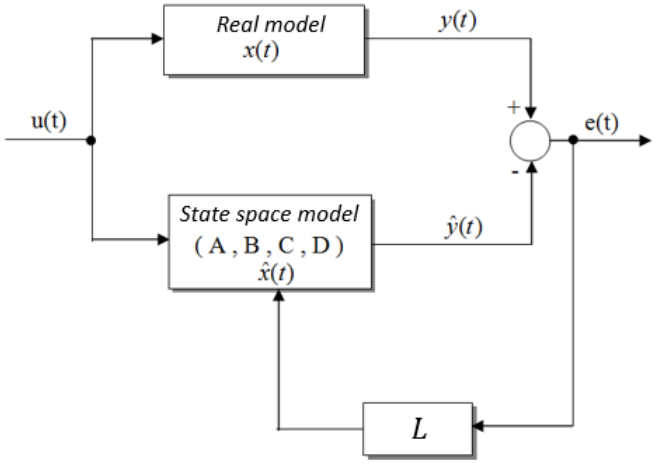

Figure 4.19: Feedback action

measurements, despite the presence of noise. The observer is derived by a statistical analysis of the system. As in [21], let us consider a discrete-time linear system with the following dynamic:

$$x[k+1] = Ax[k] + Fv[k] \tag{4.5.6}$$
$$y[k] = Cx[k] + w[k], \tag{4.5.7}$$

with $v[k]$ and $w[k]$ Gaussian white noises of the process, complying with:

$$E\{v[k]\} = 0 \qquad E\{w[k]\} = 0 \tag{4.5.8}$$
$$E\{v[k]v^T[j]\} = \begin{cases} 0 & k \neq j \\ R_v & k = j \end{cases} \qquad E\{w[k]w^T[j]\} = \begin{cases} 0 & k \neq j \\ R_w & k = j \end{cases} \tag{4.5.9}$$

$$E\{v[k]w^T[j]\} = 0. \tag{4.5.10}$$

where $E\{v[k]\}$ is the expecting value of $v[k]$, $E\{v[k]v^T[j]\}$is the correlation matrix and R_v, R_w are the covariance matrices.
Let us assume that the initial condition is also a Gaussian variable with expected value equal to the initially estimated, and with matrix of covariance P_0.
At this point, the aim is to determine the state estimation $\hat{x}[k]$, which minimizes the average quadratic error $E\{(x[k] - \hat{x}[k])(x[k] - \hat{x}[k])^T\}$. The following observer is constructed:

$$\hat{x}[k+1] = A\hat{x}[k] + Bu[k] + L[k](y[k] - C\hat{x}[k]), \tag{4.5.11}$$

$\hat{x}[k+1]$ denotes the state estimation at a time $t = (k+1)$. The output information was used to define the estimate, in that instant of time, similar to what is shown in figure 4.19.

In the previous equation, the Kalman gain L, which minimizes the average quadratic error, is given by:

$$L[k] = AP[k]C^T(R_w + CP[k]C^T)^{-1} \tag{4.5.12}$$

where,

$$P[k+1] = (A - L[k]C)P[k](A - L[k]C)^T + FR_vF^T + L[k]R_wL^T, \tag{4.5.13}$$

with $P[0] = P_0$.
The demonstration of the derivation of the optimal gain value L goes beyond the scope of this Thesis; for a more complete treatment, please review [21].
Figure 4.20 represents the comparison between the rotor speed measurements of the BLDC motors with (continuous line) and without (dotted lines) the use of the Kalman filter. The quality of the filtered data is better than the instantaneous values outgoing directly from the rotary encoders.

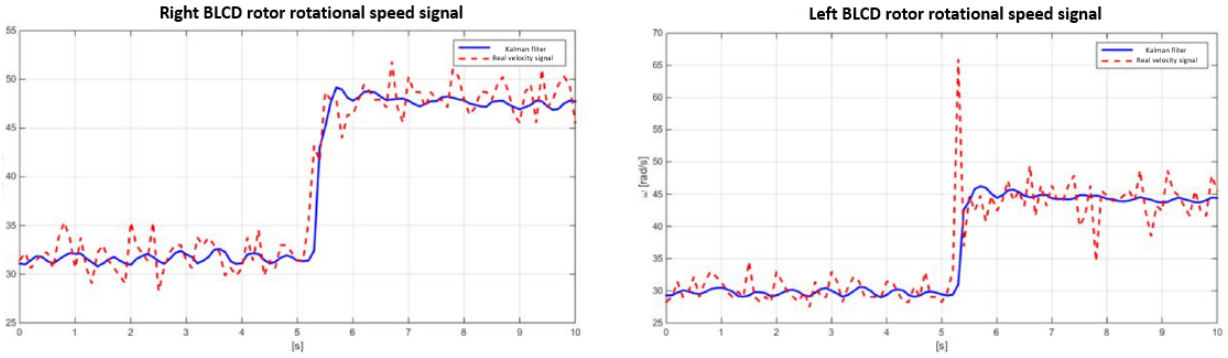

Figure 4.20: Comparison between the real rotors rotational speed signals and those filtered by means of the Kalman Filter

CHAPTER 5

Experimental results and Conclusions

Firstly, this chapter describes the methodology used to carry out the experimental tests, necessary to validate the correct functioning of the algorithm, and subsequently, it presents the results obtained, along with the relevant conclusions.

5.1 Experimental scenario

With the purpose of validate of the designed control algorithm, an experimental scenario consisting of two straight lines and two curves with constant radius was set up; it is shown in figure 5.1. On one of the two curves was simulated a section with a different coefficient of adhesion using a plastic cloth wet with soapy water. A red fixed-width line traced on the road surface defined the path.

Figure 5.1: Experimental scenario

Two experimental tests were performed with the aim of:

- validate the cruise and side slip control algorithm under slip constraints on curve manoeuvres;
- compare the results obtained using the classic cruise control algorithm and those obtained using the innovative cruise control proposed.

The control parameters have been set using the *Trial&Error* technique.
By using this method, the following values have been found for the gains of the proportional integral control, based on fuzzy logic and implemented on the BLCD motors:

- Friction-Brake: $K_p = 0,5; K_i = 0,01; K_a = 0,1;$
- Throttle: $K_p = 2; K_i = 0,05; K_a = 0,1.$

The threshold for the "Friction-throttle" step was set at 99%.
While, for the longitudinal reference generator ω_l and differential ω_d, obtained using a feed forward proportional integral control, the gains were:

- longitudinal reference: $K_p = 30; K_i = 0,1; K_a = 0,1; K_r = 30.$
- differential reference: $K_p = 3,75; K_i = 0,1; K_a = 0,1; K_r = 3,75.$

The model used for the measurements, acquired and filtered by the Kalman filter, and the discretization of equation [4.5.2], have detected the following real dynamic system:

$$\begin{bmatrix} x_1 \\ x_2 \\ x_3 \end{bmatrix}[k+1] = \begin{bmatrix} 1 & T_c & 0 \\ 0 & 1 & T_c \\ 0 & 0 & 1 \end{bmatrix} x[k] + \begin{bmatrix} 1 & 0 & 0 \\ 0 & 1 & 0 \\ 0 & 0 & 1 \end{bmatrix} v[k], \tag{5.1.1}$$

where $T_c = 0,004s$ is the sampling time. The covariance matrices of measurement errors v and w are:

$$\textit{Encoder} \qquad R_v = \begin{bmatrix} 0,001 & 0 & 0 \\ 0 & 0,01 & 0 \\ 0 & 0 & 0,1 \end{bmatrix} \quad R_w = \begin{bmatrix} 0 & 0 & 1 \end{bmatrix} \tag{5.1.2}$$

$$\textit{Gyroscope} \qquad R_v = \begin{bmatrix} 10 & 0 & 0 \\ 0 & 0,1 & 0 \\ 0 & 0 & 10 \end{bmatrix} \quad R_w = \begin{bmatrix} 1 & 0 & 0 & 0 \end{bmatrix}. \tag{5.1.3}$$

Regarding the autonomous driving algorithm, as already stated above, the value of the g_y point was set at $2,00$ m. The webcam had a resolution of 120x160 Pixel; so, the average width of the pattern is between $[5, 15]$ Pixel, and each Pixel is approximately $0,037$m.
The distance between the rear and front axles of the vehicle is $l_l = 0,275$ m, the distance between lateral axes $l_w = 0,12$ m, the radius of the wheel is $0,0326$ m and the distance between the centre of mass and the rear axle is $l_r = 0,12$ m.
During the tests, the maximum tracking error was $e_{max} = 0,2$ m, while for the proportional integral control presented in the block diagram in figure 4.14 the K_p gain was chosen to be equal to 1.
Finally, it was determined that the f_o, function, presented in section 3.5, which best satisfies a rapid convergence of the longitudinal slip into the security region, was:

$$f_o(\omega_l) = 0,04\omega_l - 0,2. \tag{5.1.4}$$

5.2 Algorithm validation

The experimental test, whose purpose was to validate the proposed algorithm, produced excellent results, shown in figures 5.2, 5.3, 5.4, 5.5.
The test can divided in three different phases:

- in the first phase, there is the transition from the "Friction" state to the "Throttle" state, in full agreement with the proportional integral control based on fuzzy logic presented in section 4.4.6. In figure 5.2 it is clearly observed that until instant t=4,4 s the references values ω_l and ω_d are obtained through a simple Feedforward (FF) action.

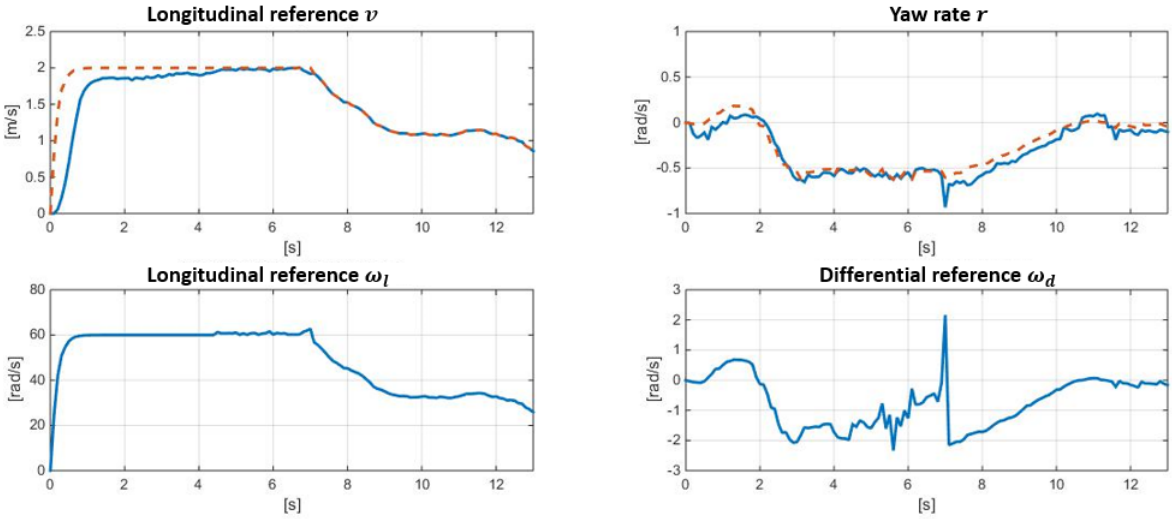

Figure 5.2: Longitudinal velocity and yaw rate with the generated references ω_l,ω_d

- once the vehicle is reaches the "Throttle" state, the second phase begins, in which the control is active. During the time interval between t=4,4 s and t=6,6 s the vehicle runs on the road surface with a near-optimal adherence. Longitudinal speed and yaw rate errors converge to zero. In practical terms, the references assigned by the "Driver" are reached; in fact, once again in figure 5.2, it can be noted that the speed v reaches the set value of 2 m/s, while the yaw rate reaches the reference r^*, in accordance with the equation 3.3.13.

- finally, a sudden change of the road conditions is visible around the instant t=7,0 s about half way during the curve manoeuvre. The decrease of the tire-road adhesion coefficient $\mu^{[1]}$ causes a sudden increase in the longitudinal slip of the left wheel, visible in figure 5.3. In this last phase, an automatic reference generator under slip constraints replaces the FF-PI control. The reference ω_l is automatically decreased and ω_d is obliged to satisfy the kinematic trajectory in open chain, as shown in figure 5.2. As a result, the longitudinal slip is quickly reduced to a safe value.

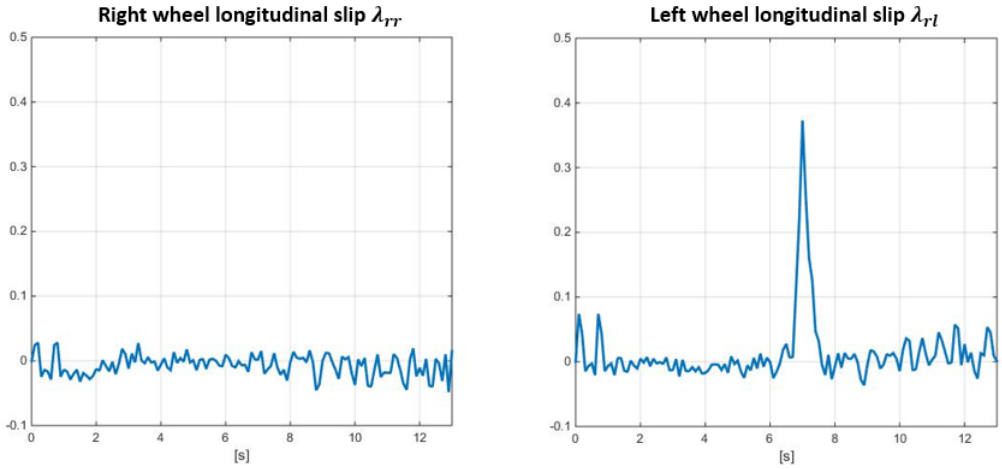

Figure 5.3: Rear wheels longitudinal slip

During the curve manoeuvre, the autonomous driving algorithm based on webcam sets a steering angle δ between of -4 and -5 degrees starting from t=2 s to t=10 s, and shown in figure 5.4.

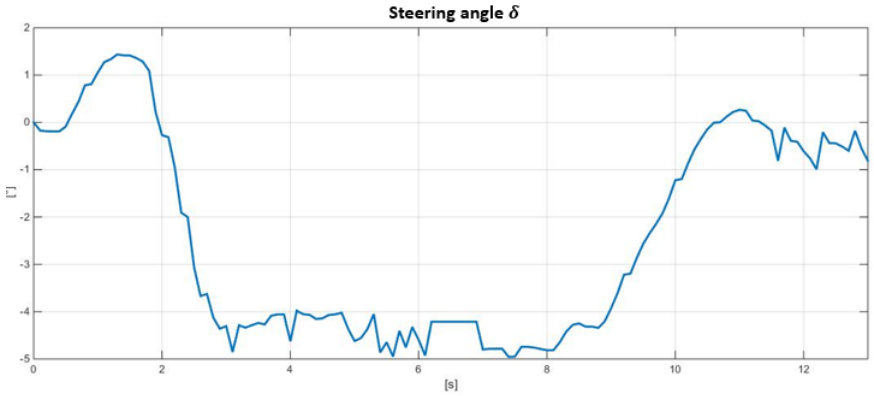

Figure 5.4: Forward wheels steering angle δ

5.3 Comparison

A second test was performed; the slip constraints been removed and only the FF-PI control that generates the references for the BLDC engines was maintained. The reference scenario was the same circuit with two straights lines and two curves with a different coefficient of adhesion between tires and road surface. The longitudinal speed reference was set to 2 m/s.

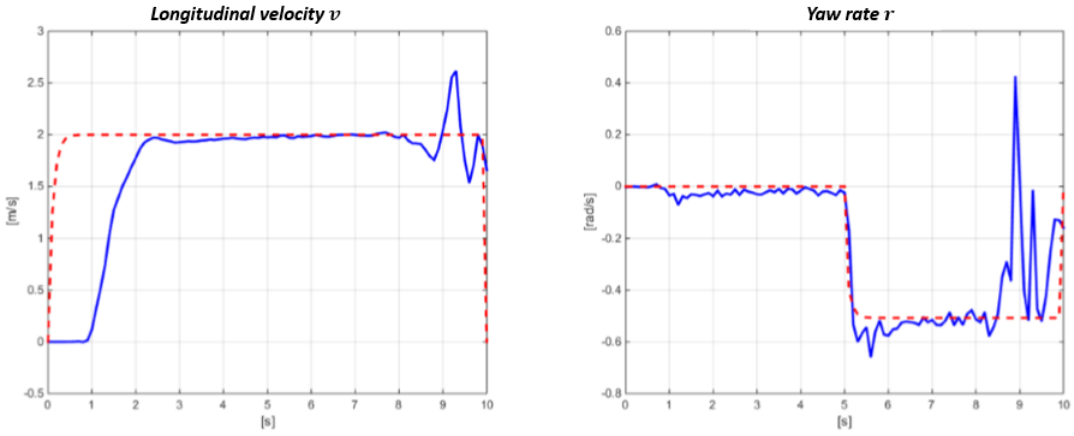

Figure 5.5: Longitudinal velocity and yaw rate, without slip constraints

Changes of the road surface conditions were present around the instant t=8,7 s. Figure 5.5 shows the longitudinal speed and yaw rate. When the longitudinal slip degenerates, the control is no longer able to manage and regulate the two speeds, leading to instability of the system. This was also affected the BLDC engines, which were no longer able to follow the references values given by the control, about the longitudinal speed and yaw rate, as shown in figure 5.6. Finally, the longitudinal slips on left and right rear wheels was not reduced to a safe value, as shown in figure 5.7.

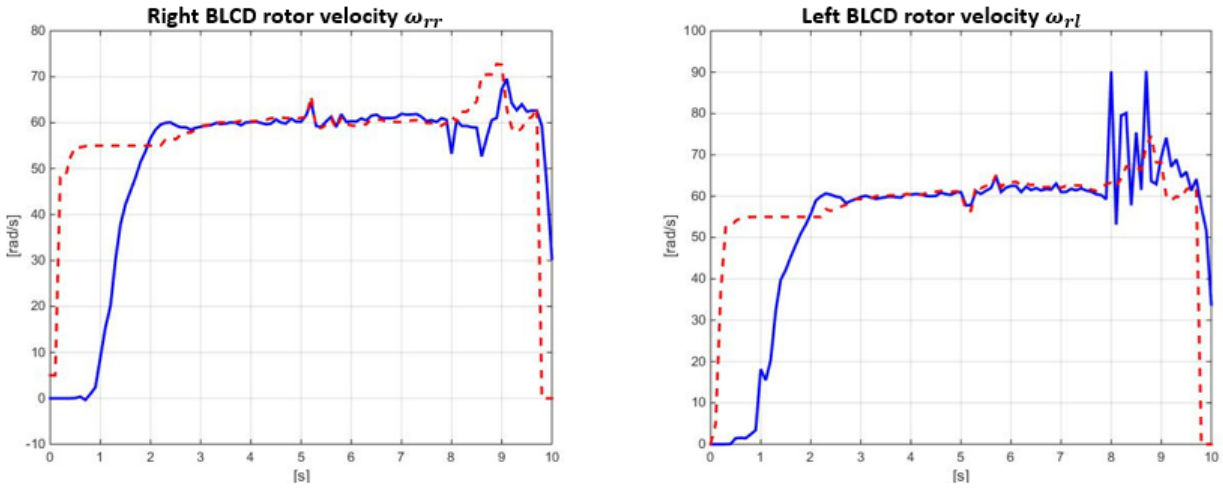

Figure 5.6: BLCD rotor velocities, without slip constraints

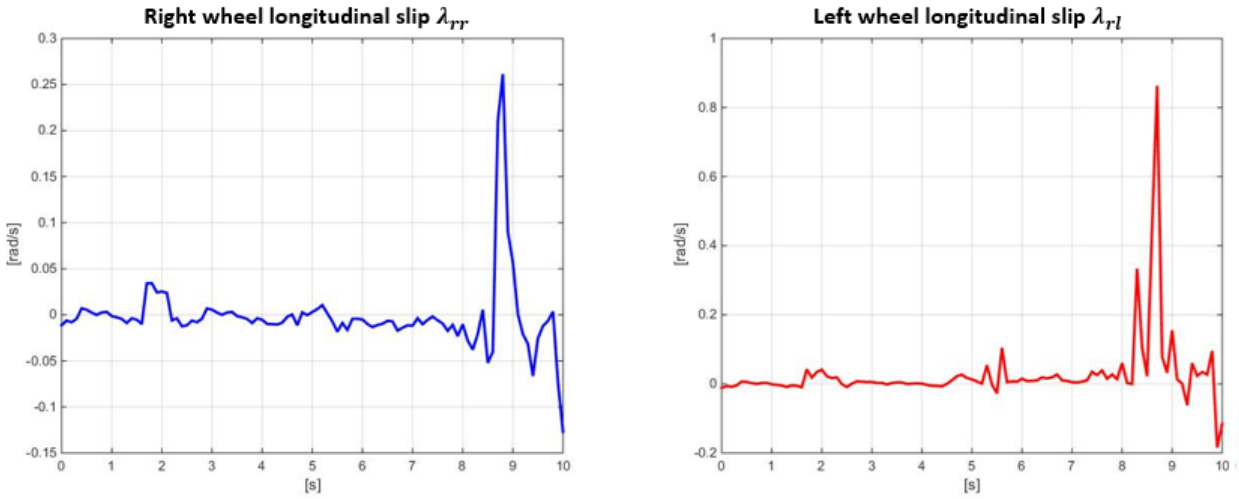

Figure 5.7: Rear wheels longitudinal slip, final test

5.4 Conclusions

It is possible to conclude that the objectives initially proposed were reached. A careful analysis was carried out on the proposed innovative algorithm for the automatic control generation in the event of slip; mechanical changes were made on a car model to test the validity of the project; also, a valid program has been implemented to meet all the specific requirements.
At the end of the research, it is possible to affirm that the standard cruise control algorithm, although widely used and known in the literature, is efficient during standard situations but has limitations during difficult external conditions.
The innovative algorithm implemented in this thesis is very versatile.
During standard conditions maintains all the advantages of a traditional cruise control; but is also able of slip monitoring, and to adapt itself to any slip changes, taking full advantage of the potential new in-wheel technology and by this mean ensuring the passengers safety.

Bibliography

[1] Y. Hori, *Future Vehicle Driven By Electricity And ControlResearch On Four-Wheel-Motored*, 'UOT Electric March II', IEEE Trans. Ind.Electron., vol. 51, no. 4, pp. 954962, Oct. 2004.

[2] M.Reichhartinger, M.Horn, *Robust Cascaded Automatic Cruise Control Of Electric Vehicles*, Int. J. Robust Nonlinear Control, vol. 26 no.4, 662-680, 2016.

[3] Y.Luo, T.Chen, S.Zhang, and K.Li, *Intelligent Hybrid Electric Vehicle ACC With Coordinated Control of Tracking Ability*, Fuel Economy, and Ride Confort, IEEE Trans. Intell. Transp. Syst., vol. 16, no.4, 2015.

[4] J.E.Naranjo, C.Gonzalez, R.Garcia, and Teresa de Pedro, *ACC+Stop&Go Maneuvers with throttle and Brake Fuzzy Control*, IEEE Trans. Intell. Transp. Syst., vol. 7, no.2, 2006.

[5] Y.Chen and J.Wang, *Adaptive Vehicle Speed Control With Input Injection for Longitudinal Motion Independent Road Frictional Condition Estimation*, IEEE Trans. Intell. Transp. Syst., vol. 60, no.3, 2011.

[6] V.L.Bageshwar, W.L.Garrard, and R.Rajamani, *Model Predictive Control of Transitional Maneuvers for Adaptive Cruise Control Vehicles*, IEEE Trans. Intell. Transp. Syst., vol. 53, no.5, 2004.

[7] C.Desjardins and B.Chaib-draa, *Cooperative Adaptive Cruise Control: A Reinforcement Learning Approach*, IEEE Trans. Intell. Transp. Syst., vol. 12, no.4, 2011.

[8] D. Corona and B. De Schutter, *ACC for a SMART Car: A Comparison Benchmark For MPC-PWA Control Methods*,IEEE Trans. Control Syst. Technol., vol. 16, no. 2, pp. 365372, Mar. 2008.

[9] J. Ploeg, B. T. M. Scheepers, E. van Nunen, N. van de Wouw, and H. Nijmeijer, *Design and Experimental Evaluation Of Cooperative ACC*, in Proc. 14th Int. IEEE Conf. Intell. Transp. Syst.,2011, pp. 260265.

[10] T. Stanger and L. del Re, *A Model Predictive Cooperative ACC Approach*,in Proc. Amer. Control Conf., 2013, pp. 13741379.

[11] B. Subudhi and S. S. Ge, *Sliding-Mode-Observer-Based Adaptive Slip Ratio Control For Electric and Hybrid Vehicles*, IEEE Trans. Intell. Transp. Syst., vol. 13, no. 4, pp. 16171626, Dec. 2012.

[12] M. Yamada, K. Ueda, I. Horiba, and N. Sugie, *Discrimination of the Road Condition Toward Understanding of Vehicle Driving Environments*, IEEE Trans. Intell. Transp. Syst., vol. 2, no. 1, pp. 2631, Mar. 2001.

[13] H.-G. Wahl, K.-L. Bauer, F. Gauterin, and M. Holzäpfel, *A Real-Time Capable Enhanced Dynamic Programming Approach for Predictive Optimal Cruise Control in Hybrid EV*, in Proc. 16th Int. IEEE Conf. Intell. Transp. Syst., 2013, pp. 16621667.

[14] M. Doumiati, A. Victorino, and A. Charara, *Dynamics Control of an In-Wheel Electric Vehicle with Steer By-Wire*, in Proc. IEEE 17th Int. IEEE Conf. Intell. Transp. Syst., 2014, pp. 348353.

[15] R.Marino,S.Scalzi,P.Tomei, and C.M.Verrelli, *Fault-tollerant Cruise Control of Electric Vehicle with Induction Motors*, Control Eng.Pract., vol.21,no.6,pp.860-869,2013.

[16] R.Marino, L.Pasquale, S.Scalzi, and C.M.Verrelli, *Automatic Rotor Speed Reference Generator for Electric Vehicles Under Slip Constraints*, IEEE Trans. Intell. Transp. Syst.2013.

[17] P. Ferraris, A. Vagatti, and F. Villate, *PM Brushless Motor Drives: A Self-Commutating System Without Rotor-Position Sensors*, in Proc. 9th Annu. Symp. Incremental Motion Contr. Syst., Devices, June 1980, pp. 305-312.

[18] S. Ogasawara and H. Akagi, *An Approach to Position Sensorless Drive for BLDC Motor*, in IEEE-IAS Conf Rec., 1990, pp. 443-447.

[19] Gwo-Ruey Yu and Rey-Chue Hwang, *Optimal PID Speed Control of Brushless DC Motors Using LQR Approach*, 2004 IEEE International Conference on Systems, Man and Cybernetics.

[20] P. Thepsatom , A. Numsomran, V. TipsuwanpoM and T. Teanthong, *DC Motor Speed Control using Fuzzy Logic based on LabVIEW*, SICE-ICASE International Joint Conference 2006 Oct. 18-2 1, 2006 in Bexco, Busan, Korea.

[21] Karl Johan Astrom,and Richard M.Murray, *Feedback Systems, An Introduction For Scientists and Engineers*, Version v2.10b (February 22, 2009).

[22] J.M.Snider, *Automatic Steering Methods for Autonomous Automobile Path Tracking*, Robotics Institute Carnegie Mellon University Pittsburgh, Pennsylvania, 2009.

[23] B.Tabbache, A.Kheloui,and M.E.H.Benbouzid, *An Adaptive Electric Dierential for Electric Vehicles Motion Stabilization*, IEEE Transactions on Vehicular Technology, 60: 104-110, 2011.

[24] H.Du.N.Zhang, and F.Naghdy, *Velocity-Dependent Robust Control for Improving Vehicle Lateral Dynamics*, Transportation Research Part C, 19: 454-468, 2011.

[25] F.Tahami,R.Kazemi,and S.Farhanghi, *A Novel Driver Assist Stability System for All-Wheel-Drive EV*, IEEE Transactions on Vehicular Technology, 52: 683-692, 2003.

[26] P.Tomei, and C.M.Verrelli, *A Monlinear Adaptive Speed Tracking Control for Sensorless Permenent Magnet Step Motors with Unknown Load Torque*, International Journal of Adaptive Control and Signal Processing, 22:266:288, 2008.

[27] M. Reed and B. Simon, *Functional Analysis*, vol. 1, San Diego, CA, USA: Academic Press, 1980, ser. Methods of Modern Mathematical Physics.

[28] R.Marino,P.Tomei,and C.M.Verrelli, *Induction motor control design*, Berlin,Germany: Springe-Verlag,2010.

[29] A.El Magri et aol., *Sensorless Adaptive Output Feedback Control of Wind Energy Systems with PMS Generators*, Control Eng. Pract., vol.21, no. 4, pp. 530-543,2013.

[30] E. Kreyszig, *Introductory Functional Analysis with Applications*, Hoboken, NJ,USA:Wiley,1978.

[31] R.Marino, S.Scalzi, P.Tomei, and C.M.Verrelli, *Fault-Tollerant Cruise Control of Electric Vehicle with Induction Motors*, Control Eng.Pract., vol.21,no.6,pp.860-869,2013.

[32] R.Marino,and C.M.Verrelli, *A Global State Feedback Output Regulating Control for Uncertain Systems in Strict Feedback Form*, Syst.Control Lett.,vol.58,no.9,pp.682-690,Sep.2009.

[33]The Automotive Century: Most Influential People, Ferdinand Porsche, *http://www.autohistory.org/feature_6.html*, August 2000, accessed 25th July 2010

[34]Lohner-Porsche Mixte Voiturette, *http://www.ultimatecarpage.com/pic/3456/Lohner-Porsche-Mixte-Voiturette_2.html*, November 2007, accessed 25th July 2010

[35] *https://www.google.com/patents/US2519859?dq=ininventor:%22Ralph+R+Teetor%22&hl=en&sa=X&ei=mZ9kVKHAIJfSoASgsoC4CQ&ved=0CGwQ6AEwCw*

[36] *https://www.google.com/patents/US5454442*

[37]. Pacejka H.B.,*Tyre and Vehicle Dynamic*, Elsevier, ISBN 9780750669184, 2006.

[38] Adams/Tire User Manual, *Using the PAC2002 Tire Model* .

[39] M. Reed,and B. Simon.*Functional Analysis*, Vol. 1 (Methods of Modern Mathematical Physics). Academic Press, Elsevier, 1980

[40] National Instruments, *NI myRIO user guide and specifications*, 2013